WAVE PROPAGATION IN DISPERSIVE WEB MEDIA

By

SUEFEN CHEN

Bachelor of Science
Chinese Culture University
Taipei, Taiwan
1984

Master of Science
Oklahoma State University
Stillwater, Oklahoma
1986

Submitted to the Faculty of the
Graduate College of the
Oklahoma State University
in partial fulfillment of
the requirements for
the Degree of
DOCTOR OF PHILOSOPHY
December, 1992

OKLAHOMA STATE UNIVERSITY

WAVE PROPAGATION IN DISPERSIVE WEB MEDIA

Thesis Approved:

R L Lowery
Thesis Advisor

P M Morel

J. K. Good

C D Latimer

Thomas C. Collins
Dean of the Graduate College

ACKNOWLEDGMENT

Many thanks are due to all the people who helped me to accomplish this work. I would like to thank my major advisor, Dr. Lowery, for guiding and helping me through this research work. Because of his knowledge in instrumentation and measurement, he leads me into this field. I enjoy learning everything and am thankful to God for giving me this chance. It has been a wonderful time of learning and experience for me ever since I got into mechanical and aerospace department. I am also indebted to Dr. Moretti. Thank you for helping me through and backing me up. I thank him for giving me so many opportunities to learn and to be trained. I appreciate everything that he has done in my life. I would also like to express my appreciation to Dr. Good. I thank him for encouraging me, for providing me laboratory equipment, and for giving many helpful suggestions. I am also thankful to Dr. Latino for his concern about my work and his encouragement.

Special thanks are due to all the faculty and staff in the MAE department of Oklahoma State University. I am grateful to have all of their unforgettable friendship. I thank all for encouraging me to continue my degree work. I enjoyed my stay and learned so much in this department. Thanks are also extended to the Web Handling Research Center

and the MAE department for the financial support which enabled me to earn this degree.

I also need to thank my husband, Minter Cheng for his love, encouragement, and support. I thank him for his help in my study and research work. I thank him for providing suggestions and ideas. My parents, parents-in-law, sisters, brother, and in-laws are appreciated for their understanding, financial support, and constant encouragement. Many thanks are also due to all my friends: Tom & Sue Moore, Johanna, Anne, Jackie, Judy, and Mark Simpkins. There are many others I would like to thank but forgive me if I do not mention your name.

I can not express my thanks well enough. I just thank God for all of you in my life. Without all of you, I could not reach this point. I will miss all of you and Stillwater.

TABLE OF CONTENTS

Chapter page

LIST OF TABLES

LIST OF FIGURES

Figure Page

Figure Page

NOMENCLATURE

a	radius of a circular membrane, m
A	arbitrary constant
b	width of web, m
c	light velocity in vacuum, m/sec
C	speed of sound in air, m/sec
e	charge, coulomb
E	Young's modulus, N/m^2
f	frequency, Hz
f_n	natural frequencies, Hz
f, f_1, f_2	arbitrary functions
F	applied force, N
F_ω	reactive force due to air-loading, N
h	thickness of plate, m
I	moment of inertial, m^4
J_1	Bessel function of the first order
k	wave number of air, $k = \omega/C = 2\pi/\lambda$
K	wave number of membrane, $K = \omega/V_{ph}$
m	mass of oscillating particles, Kg
n	integer
p	air pressure, N/m^2
P	amplitude of air pressure, N/m^2
q	attenuation constant in air
N_e	number of particles per volume

S	cross-sectional area, m^2
r	distance, m
t	time, sec
$\mathbf{t}$	non-dimensional time, t-x/C
T	tension of web, N
T_1	tension of web per unit length, N/m
V	velocity of flexural wave along ribbon, m/sec
V_m	velocity of flexural wave along membrane, m/sec
V_p	velocity of flexural wave along plate, m/sec
V_g	group velocity, m/sec
V_{ph}	phase velocity, m/sec
x,y	spatial coordinates, m
ε	dielectric constant
η	displacement from equilibrium line, m
$\mathbf{l}$	length of ribbon or string, m
φ	function
κ	radius of gyration of cross section
λ	wave length, m
μ	index of refraction
ν	Poisson's ratio
θ	incident angle between pulser tube and web, degree
ρ	air density, kg/m^3
σ_1	mass per unit length, Kg/m
σ_2	areal density of web, Kg/m^2
σ_3	density of web, Kg/m^3
τ	period, sec
ω	angular frequency, rad/sec

ξ	constant, $N_e e^2/m/2C$
ζ	damping constant

CHAPTER I

INTRODUCTION

1.1 Runnability Disturbances and Web Tension

It has long been recognized that web breaks, color register errors, web flutter, and wrinkles are the most important runnability disturbances of web handling processes. These disturbances will cause both material and time waste. Most of all, they might cause a fatal delay in delivery. From previous researchers' observations, web tension or tension variations have strong effects on runnability properties. Tension is the pulling force applied to a running web. In the ideal case, the tension should be evenly distributed across the whole web width, but in practice this is usually not the case. How to find a better way to measure tension and eliminate these disturbances has been an important problem.

With the arrival of high-speed web machines and winders, improving the quality in the control process of web handling industries is important. In other words, providing accurate and continuous tension profiles of cross machine direction throughout the whole process (time records) is needed. The conventional tension meter is a load-cell type. This type of

tension meter can only measure mean tension values of the whole web width. It does not provide local tension information. Up to last decade, new techniques have made it possible to measure the tension distribution. These new tension meters are either very large or else hand-held devices.

1.2 Point-Source Process

One new technique, the point-source process, is being developed at Oklahoma State University and sponsored by the Web Handling Center. This process is different from others by its unique excitation method. The point-source system has a very compact measuring head so it can be used in situations where little space is available.

This process uses air pulses to generate a short-duration wave into a web and measures the time-of-flight between two sensors. It also determines the wave velocity traveling in a web, and calculates a web's local tension with additional information such as web density, width, thickness, and Young's modulus. Determination of the phase velocity of the wave is the hardest part in this process because the pulse wave traveling along the web keeps changing its shape. Even by using the cross-correlation method, determining a wave velocity is still not an easy task. In addition, it is very time consuming.

1.3 Objective

The ultimate objective of this research is to improve the point-source process so it can also work with thicker material. A study of the mechanics of wave motions in webs was therefore undertaken to achieve this objective. The experiments were conducted on a stationary setup with various types of webs. Point-source and loudspeaker systems were used as wave exciters. Sensors included Electret and B&K microphones, OPTEK sensors, and a laser vibrometer. To achieve the above objectives, the approaches in this study were as follows:

1. To change pulser tube orientation and see the effects on wave forms at various tensions.
2. To learn the basic concepts from a single frequency propagation generated by a loudspeaker system.
3. To understand the dispersion of wave propagation in point-source system by studying a pseudo square wave pulse with frequency decomposition.
4. To take the stiffness into account by modifying an existing model; and to investigate the effect of air load on the traveling wave velocity.
5. To evaluate how well each model can predict tension by comparing it with "known" tension (dead weight).
6. To check whether the first order Bessel function from the theory in optics represents a similar shape of forerunners as obtained in the experiments.

7. To learn whether the forerunner waves are created by the air blast from the point-source system by comparing air blast results with a mechanical excitation method.

1.4 Present Contribution

The experimental observations strongly suggest that the pulser tube should be arranged in either cross direction or machine direction. For a direct air pulse into a web, the wave forms were affected not only by an acoustical shock wave but also by aerodynamic effect. Tests on various types of webs show that the point-process works very well with a wide range of materials. A tensioned-plate model with air loading was derived but experimental results show that the calculated tensions are always higher than the "known" tension.

1.5 Outline of Report

The first chapter of this five-chapter report is the introduction which describes runnability disturbances and their relationship to web tension. The objectives of this study are also stated and justified. Chapter II gives a literature survey of web tension meters. Wave equations are also given for the ribbon, beam, membrane, stiffness string or tensioned beam, and plate models. A description of forerunners in optics, and precursors in piano strings is also presented. Chapter III describes the complete experimental facility, including the point-source system,

loudspeaker system, sensors, testing materials, and stiffness experimental setup. The experimental data and plots from the study are discussed thoroughly in Chapter IV. Chapter V gives the conclusions from the work and recommendations for future work.

CHAPTER II

LITERATURE REVIEW

The literature regarding web-tension meters has been extensively surveyed. Inclusion of noteworthy results is in section 2.1 where the emphasis is on dynamic and local tension measurements. Section 2.2 is a review of dispersion, phase velocity, and group velocity. Individual discussions on the wave equations for ribbon (string), membrane, beam, plate, and stiff string or tensioned beam models are in sections 2.3 through 2.7. Since the point-source process requires the information of the velocity of a pulse wave traveling in the web, the focus of attention in each model is the relationship between tension and velocity. Section 2.8 addresses the effects of a point force on a string or a membrane. Experimental results clearly show the presence of forerunners (precursors) in the amplitude-time plots; therefore, background information about forerunners in optics (Sec. 2.8) and precursors in a piano string (Sec. 2.9) are also reviewed.

2.1 Web Tension Measuring Principles and Devices

The conventional way of measuring web tension is by

using load cells mounted on roller bearings. These type of tension meter can only give the mean tension value of the whole web width but does not give any indication about uneven tension distribution or local tension peaks. To achieve better control of a web handling process, advanced web tension meters having the ability of measuring local and dynamic web tensions are desirable.

Tidningspapersbrukens Fordkningslaboratorium (TFL) in Sweden developed a device involving an acoustic chamber (1,2). Measurements of the amplitude of the web determines its tension, where as a loudspeaker generates an acoustic wave at the measuring head. This device can measure tension variations and record cross-direction (CD) tension profiles.

The Altim Tensometer is an acoustic and non-contacting tension meter, marked by Altim Control Company (1-4). A loudspeaker induces a wave into a web. The wave propagates in the machine direction and its velocity depends on applied tension. With two microphones placed on each side of the sound source as sensors, double measurements in both directions cancel out the web's speed. Then by employing the cross-correlation method and advanced digital signal processing techniques, the Tensometer can obtain the wave velocity. With calibration data, local tension and a tension profile of the web can be drawn. However, this device is no longer in production.

STFI's web tension indicator made by Swedish Forest Products Research Laboratory also uses a loudspeaker to

vibrate a web (5). However, it measures tension by relating the tension to resonant frequency which increases with increasing tension. Adjusting the phase difference between input and output signals in this vibrating system controls and holds the resonant frequency. Then, based on the vibrating string formula (discussed in section 2.3), one can calculate the tension.

The Norwegian Pulp and Paper Research Institute have constructed a portable and hand-held tension meter (2,4,6). This device consists of a curved steel blade which is pressed into a moving web causing the web to indent 1 to 2 mm. Calibration curves convert tension based on the depth of the blade's indentation, which is measured by a non-contacting inductive transducer. Even though this device is a simple, light weight, low-cost, portable, and one-man operated tension meter, it is only good for troubleshooting and not practical for monitoring because of not providing continuous tension profiles.

The principle used in the Altim Tensometer has been further developed and applied in a new meter, Tenscan, by ABB Stromberg Drives Oy (4,7,8). This system uses three optical sensors (sensitive semiconductors) instead of a pair of microphones. It also requires calibration measurements of wave velocity and tension for different basis weights, which are programmed into the system memory. The Tenscan is also a non-contacting tension meter and can measure the CD distribution of tension in a moving paper web. Both the

Tensometer and the Tenscan have big measuring heads and must be either attached or mounted to traverse mechanisms.

Another tension meter blows compressed air into an inverted cavity over a web (2,7). Scandev Invent Beetle converts the back pressure under the cavity into web tension. However, the disadvantages of this device are that measurements near the web's edge are not possible and the back pressure is affected by temperature and humidity.

A joint effort by Valmet Paper Machinery and Davy Mckee Limited has been made to adapt an existing technique of metal sheet industries to measure CD tension variation in a wide paper web (9). Originally, Davy Mckee developed the Vidimon Shapemeter to measure the flatness of metal based on the relationship between shape and the tension distribution in the production (10). However, the two companies redesigned the Shapemeter by adding an air-lubricated bearing (all web surfaces float on an air film) and modifying it with greater electronic amplification. This way they achieved sufficient pneumatic output signals for flatness measurements in a paper web. Converting a single roller to a multi-section roller they were able to generate a CD tension profile.

2.2 Dispersion, and Phase and Group Velocities

When a wave is composed of different frequency components which travels at different velocities (the change in wave shape), is called dispersion (11,12). In this

situation, higher frequency waves travel faster than lower frequency ones. Consider a simple combination of two waves with different angular frequencies and wave numbers. These two waves are superimposed on each other and can be expressed as (13,14)

$$\varphi = A \cos (\omega_1 t - k_1 x) + A \cos (\omega_2 t - k_2 x)$$

Using the sum and product of the trigonometric functions, one obtains the following equation

$$\varphi = 2A \cos (\omega t - kx) \cos (\Delta\omega t - \Delta k x)$$

where

$$(\omega_1 - \omega_2)/2 = \Delta\omega \qquad (k_1 - k_2)/2 = \Delta k$$

$$(\omega_1 + \omega_2)/2 = \omega \qquad (k_1 + k_2)/2 = k$$

Then, the group velocity (V_g) (which is the velocity of transmission of slowly varying modulations of a harmonic wave) is given by

$$V_g = \frac{\Delta\omega}{\Delta k} \rightarrow \frac{\partial\omega}{\partial k} \qquad \text{for} \qquad \Delta k \rightarrow 0$$

and the phase velocity (V_{ph}) (or so-called carrier's velocity) is given by

$$V_{ph} = \frac{\omega}{k}$$

These two velocities can be related by

$$V_g = V_{ph} + k\frac{\partial V_{ph}}{\partial k} \qquad \text{or} \qquad V_g = V_{ph} - \lambda\frac{\partial V_{ph}}{\partial \lambda}$$

Energy is transmitted at the group velocity in most physical systems. In a dispersive medium, phase velocity is no longer the same as group velocity. The phase velocity

often depends not only on the wave frequency but also on the density of the medium. If a finite signal is deformed as it travels along the medium, defining its velocity becomes even harder on account of the changing shape. An absorbing medium is the best example. Generally speaking, absorption and dispersion are always associated with each other and both of them are frequency dependent.

2.3 Ribbon (String) Model

Merhaut addressed the oscillations of a thin ribbon in his *Theory of Electroacoustics* (15). Consider such a ribbon of finite length, constant width, uniform thickness, and density. Also let this ribbon be stressed by a uniform tension at both ends and placed along the x axis symmetrically as shown in Figure 1. Assume further that the ribbon is perfectly flexible and the tension is the only restoring force, neglecting the gravity and air-loading effects. No longitudinal motion of alternate compression and tension is assumed (16). The displacement of the ribbon from its equilibrium position is $\eta(x,t)$. Then, by applying Newton's second law to a differential section of ribbon, the equation of motion can be derived for the transverse vibration as (15):

$$\frac{\partial^2 \eta}{\partial x^2} = \frac{1}{V^2} \frac{\partial^2 \eta}{\partial t^2}$$

Its solution has the form

$$\eta = f_1(x - Vt) + f_2(x + Vt)$$

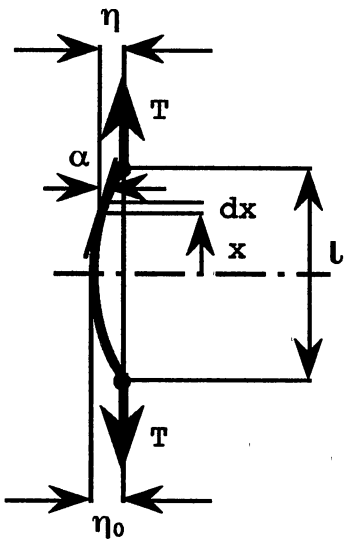

Figure 1. Side View of Ribbon (String) Vibrating in z Direction

where $V = \sqrt{T/\sigma_1}$ is the propagation velocity of flexural waves along the ribbon (String) in the x direction. Note V is a constant here. Rewriting $V = \sqrt{T/\sigma_1}$ for tension as

$$T = \sigma_1 V^2$$

The natural frequencies (f_n) of the ribbon are

$$f_n = \frac{n}{2\ell}\sqrt{\frac{T}{\sigma_1}}$$

which is essentially the same formula applied on STFI's tension indicator.

2.4 Membrane Model with Air-Loading

Wave propagation in a thin membrane under uniaxial tension (17,18) in one-dimension will have the same wave

equation as that of a ribbon. In the previous section, the air-loading effect is neglected which is valid only in a vacuum. However, in the atmosphere, the pressure of surrounding air on the membrane produces a reactive force (F_ω) which acts as a mass load. The equation of motion can be modified with an additional air-loading term (F_ω) as

$$\sigma_2 \frac{\partial^2 \eta}{\partial t^2} = T_1 \frac{\partial^2 \eta}{\partial x^2} + F_\omega$$

Then, by applying the general wave equation in air and also applying the continuity of traverse velocity of a membrane equal to that of the air particle on the membrane surface, the wave equation can be solved to give tension

$$T_1 = \left(\sigma_2 + \frac{2\rho}{\sqrt{K^2 - k^2}} \right) V_{ph}^2$$

Detailed rederivation is shown in Appendix A. Wave propagation in this case is dispersive, i.e. if the wave is not a single frequency one, then its shape is not retained.

For a rectangular membrane with even tension around its edge, the 2-dimensional equation of motion is (16,19)

$$\frac{\partial^2 \eta}{\partial x^2} + \frac{\partial^2 \eta}{\partial y^2} = \frac{1}{V_m^2} \frac{\partial^2 \eta}{\partial t^2}$$

where

$$V_m = \sqrt{T_1/\sigma_2}$$

and its general solution for its displacement is

$$\eta = \int_0^{2\pi} f(x \cos \alpha + y \sin \alpha - V_m t)\, d\alpha$$

Each component of the integral represents a wave traveling

with velocity V_m in a direction at an angle α to the x-axis.

2.5 Beam Model

The transverse motion of a uniform cross sectional beam is assumed to be perpendicular to a neutral plane. The bending moment is a function of distance from one end of the beam. By knowing the moment and shear force relationship at equilibrium and the net force accelerating the beam's mass, the general wave equation of the beam is (12,14,19,20)

$$- E\kappa^2 \frac{\partial^4 \eta}{\partial x^4} + \kappa^2 \sigma_3 \frac{\partial^4 \eta}{\partial x^2 \partial t^2} = \sigma_3 \frac{\partial^2 \eta}{\partial t^2}$$

If the ratio of κ/l of the rod (beam) is very small, the rotary inertia term is relatively small compared with the other two terms, and it is customarily omitted (21). Therefore, the approximate wave equation becomes much simpler,

$$E\kappa^2 \frac{\partial^4 \eta}{\partial x^4} = - \sigma_3 \frac{\partial^2 \eta}{\partial t^2}$$

and its phase velocity is

$$V_{ph} = \left(\frac{4\pi^2 E\kappa^2}{\sigma_3} \right)^{1/4} \sqrt{f}$$

For a rectangular rod, $\kappa^2 = h^2/12$ if h is the thickness in the plane of vibration.

If rotary inertia is taken into account, the phase velocity is (22)

$$V_{ph} = \sqrt{\frac{E}{\sigma_3}}\, \kappa K (1 + \kappa^2 K^2)^{-1/2}$$

and the group velocity is

$$V_g = \sqrt{\frac{E}{\sigma_3}}\ \kappa K \left(2(1 + \kappa^2K^2)^{-1/2} - \kappa^2K^2(1 + \kappa^2K^2)^{-3/2}\right)$$

With increasing frequency, the phase velocity approaches the group velocity and both converge on the longitudinal wave velocity, $\sqrt{\frac{E}{\sigma_3}}$.

Since a beam is a dispersive medium (refer to section 2.6), it is very interesting to see how a beam acts on a pulse input. Morse (16,19) gives the comparison of beam and string responses as shown in Figure 2.

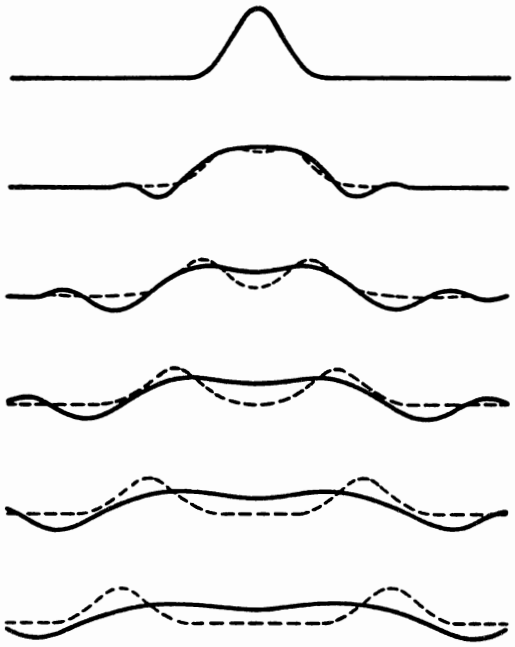

Source: Morse, P. M., Theoretical Acoustics, McGraw-Hill, 1968

Figure 2. Comparison of Beam's and String's Displacements

2.6 Plate Model

The wave motion of a plate in two dimensions is much more complex than that of a beam in one dimension. One needs to consider also the sidewise motion, bringing in Poisson's ratio which is around 0.3 for most materials. The equation of motion can be derived from the Lagrangian method (19,20).

$$\frac{\partial^4\eta}{\partial x^4} + \frac{\partial^4\eta}{\partial y^4} + 2\,\frac{\partial^4\eta}{\partial x^2\partial y^2} = \frac{12\sigma_3(1-\nu^2)}{Eh^2}\,\omega^2\eta$$

and the equivalent wave velocity in a plate is

$$V_{ph} = \left(\frac{\pi^2 Eh^2}{3\sigma_3(1-\nu^2)}\right)^{1/4}\sqrt{f}$$

The frequency dependence of phase velocity indicates that a beam and a plate are dispersing media. The group velocity is different from phase velocity and is

$$V_g = 2\,\overline{V_{ph}}$$

where $\overline{V_{ph}}$ is the phase velocity for the mean frequency in the group.

2.7 Stiff-String or Tensioned-Beam Model

There is no sharp border between a membrane (string) and a plate (beam). Generally speaking, tension is more important then stiffness as a restoring force for a membrane (string), and vice versa for a plate (beam). However, there is a range of intermediate cases from thick paper (stiff stings) to thin metal foil (tensioned beam). On one hand, Morse (16,19) describes the equation of the wave motion for a stiff string under tension is

$$T \frac{\partial^2 \eta}{\partial x^2} - E\kappa^2 S \frac{\partial^4 \eta}{\partial x^4} = \sigma_1 \frac{\partial^2 \eta}{\partial t^2}$$

On the other hand, Timoshenko (23) gives the equation of motion for a tensioned beam as

$$T \frac{\partial^2 \eta}{\partial x^2} - EI \frac{\partial^4 \eta}{\partial x^4} = \sigma_1 \frac{\partial^2 \eta}{\partial t^2}$$

Solving for tension in terms of phase velocity and angular frequency (refer to Appendix B) gives:

$$T = \frac{\sigma_1 V_{ph}^4 - EI\omega^2}{V_{ph}^2}$$

2.8 Point Force

When a point force is applied to a string or a membrane, their reactions are very different (19). The string deflects as

$$\eta = Fx(l-x)/Tl$$

The displacement of the string is finite and proportional to the force. However, a (ideal) membrane with radius, a, can not sustain a point force. No matter how small the force is, the displacement will be infinite if a force is applied at the center (r = 0), according to

$$\eta = \frac{2F}{T_1} \ln(\frac{a}{r})$$

where r is a distance from the center to the point where the force is applied. If a force is applied at edge (r = a), the displacement will be zero. In fact, these results do not happen in reality. The assumption of a force applied at a

point is too much simplification. Actually the force is over a small area of the membrane and over a small length of the string. Changing the size of the area where the force is applied does make the displacement different. A certain amount of stiffness within a membrane can also avoid producing an infinite displacement.

2.9 Forerunners in Optics

In optics, the velocity of light in vacuum divided by the index of refraction is phase velocity. Besides phase and group velocities, two more types of velocities need also be addressed. One is the signal velocity, defined by Brillouin (13) as "the velocity at which the main part of the wave motion propagates in the dispersive medium." He also stated "the signal velocity is practically the same as the group velocity when the wave motion proceeds without strong absorption." The other is the wave front velocity which progresses with the velocity of light in vacuum through a dispersive medium.

The one-end terminated wave in Figure 3 can be described mathematically as

$$f(t) = \begin{cases} 0 & t < 0 \\ \sin\frac{2\pi t}{\tau} & t > 0 \end{cases}$$

or shown in a complex integration formula as

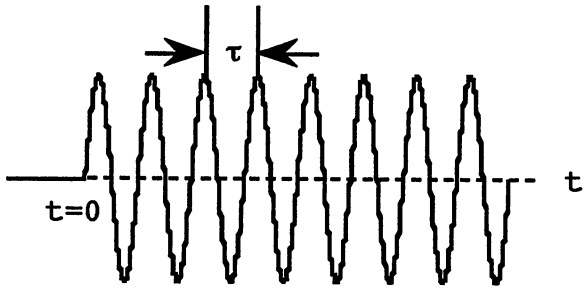

Figure 3. One-End Terminated Sinusoidal Wave

$$f(t) = \frac{1}{2\pi} \text{Re} \int e^{-i\omega t} \frac{d\omega}{\omega - \frac{2\pi}{\tau}}$$

Taking dispersion into account and rewriting the above equation one obtains

$$f(t,x) = \frac{1}{2\pi} \text{Re} \int e^{-i\omega t + ikx} \frac{d\omega}{\omega - \frac{2\pi}{\tau}}$$

where

$$k = \frac{\omega}{V_{ph}} = \frac{\omega}{\frac{c}{\mu}}$$

and

$$\mu^2 = 1 + \frac{N_e e^2/m}{\omega_0^2 - 2i\omega\zeta - \omega^2}$$

Hutchison (24) gives more detailed physics background information about the above equation.

Then, if one evaluates the integral of $f(t,x)$ by neglecting the damping ζ of the ionic oscillations (i.e. no

absorption) and defining new variables: $t = t-x/c$ and $\xi = N_e e^2/m/2c$ and he obtains the solution for small values of t/ξ .i.e. before the main signal arrives. Therefore, the forerunners can be described mathematically by

$$f(t,x) = \frac{2\pi}{\tau}\sqrt{\frac{t}{\xi}}J_1(2\sqrt{t\,\xi})$$

The initial amplitude and period of forerunners is very small, compared with the incident ones. The initial period is approximately

$$t_0 = \frac{\pi^2}{2\xi}$$

and is independent of the incident period. The amplitude and period of the forerunners keep increasing as shown in Figure 4. Finally the forerunners join on to the main signal.

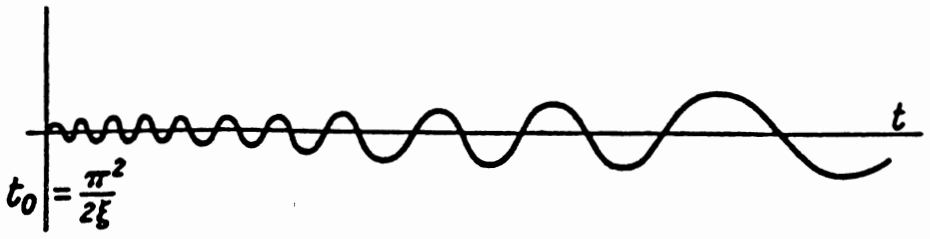

Source: Brillouin, L., Wave Propagation and Group Velocity, Academic Press, 1960 (13)

Figure 4. Schematic Diagram of Forerunners

2.10 Precursors in Piano String

The dispersion relation for transverse waves on a uniform piano string with circular cross section and flexural stiffness is given by (25)

$$\frac{ES^2}{4\pi} k^4 + Tk^2 = \sigma_1 \omega^2$$

This equation is essentially the same as the stiffness string equation in section 2.7 if $S/4\pi$ is replaced by κ^2. Solving V_{ph} in terms of tension and frequency one obtains

$$V_{ph} = \left\{ \frac{T}{2\sigma_1} + \left(\frac{T}{2\sigma_1} + \frac{ES^2 \pi f^2}{\sigma_1} \right)^{1/2} \right\}^{1/2}$$

Precursors are observed and shown in Podlesak's paper, but he has not attempted to describe precursors mathematically nor to abstract the information from the precursors.

CHAPTER III

EXPERIMENTAL FACILITY

The experimental phase of the study discussed in this report was conducted in the Web Handling Research Center at Oklahoma State University. A special stationary test stand was designed and constructed especially for this study. The main components of the setup and testing materials are described in this chapter.

3.1 Overall Experimental Setup

In this study, tension is determined from measurements of wave velocity and application of the fundamental wave equations. A "known" tension, based upon dead weights, was applied in the machine direction on the stationary test stand. Sensors were used to detect a web's motion providing voltage outputs which were then converted to two individual electronic wave forms on a HP digital oscilloscope. Both of the sensors were installed at a fixed distance either on the same side or opposite side with the pulser tube, but in succession along the wave propagation direction. The overall schematic experimental setup, shown in Figure 5, consists of four main parts: a test stand, a pulser tube, sensors, and a digital oscilloscope. The test stand is made of three 3.5-

inch-diameter plastic rollers, each 12 inches in length centered with 2-inch-diameter ball bearings. Each of the three rollers is individually mounted on a rigid steel frame. The orientation of roller number 3 can be slightly adjusted so that a testing material surface will be flat. The testing web is placed on the rollers with one end fixed and the other end weighted. Web tensions are simulated by changing the weights. In this study, the web tension was varied from 0.5

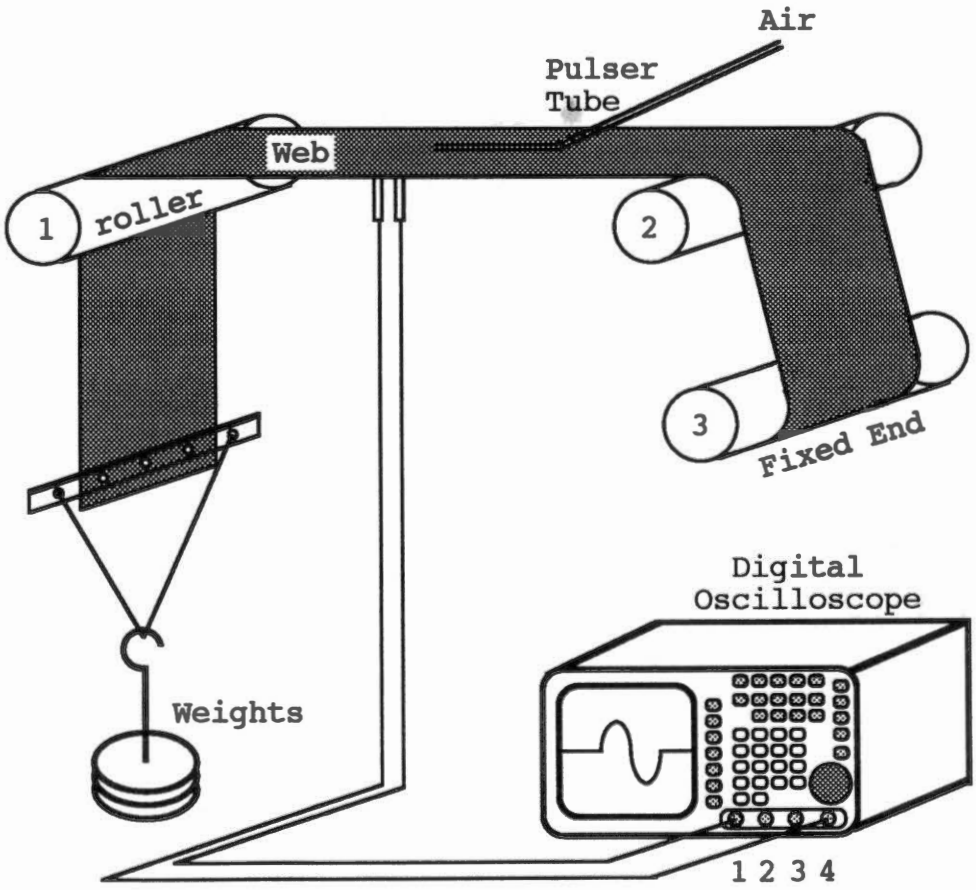

Figure 5. Overall Experimental Setup

to 2 pounds per linear inch (pli) for various type of materials tested.

A sound source with preset intervals was placed adjacent to the web. This puts spatially confined sound pulses into the testing web. Two sensors were mounted on a sensor holder connected with a precise one-dimensional traversing mechanism. This traversing mechanism can locate the sensors at desired cross-direction positions such that cross web tension profiles can be obtained. The traversing mechanism is also transportable and can be located at various machine positions. It is accurate to within 0.01 inch.

The gaps between the two sensors and the testing web are very critical for OPTEK infrared reflective sensors. Due to the web's deflection by its own weight, increasing web tension can cause the web to be away from the sensors or vice versa. Therefore, the elevation of the sensor holder needs to be adjustable. If tension is a variable and signal output is from the OPTEK sensors, then the gaps need to be adjusted to acquire the best signals. The distance between the sensors is also adjustable by using different sensor holders. Most of the time, the two sensors are set apart around 4 inches. The gap problem is not encountered with some other types of sensors.

3.2 Sound Sources

Two sound-source systems used in this study induce acoustic waves into the testing web: the point-source and the

loudspeaker systems. Full descriptions of these two systems will be addressed individually in the following sections.

3.2.1 Speaker with Tone Burst System

Figure 6 shows a schematic diagram for the loudspeaker system. Usually the function generator provides a continuous sinusoidal wave but can provide a square wave if needed. The initially continuous wave passes through the tone burst, the amplifier, and appear the output of the loudspeaker as a both-end terminated signal as shown in Figure 6. The operating frequency of the signal ranges from 0.3 to 5 KHz.

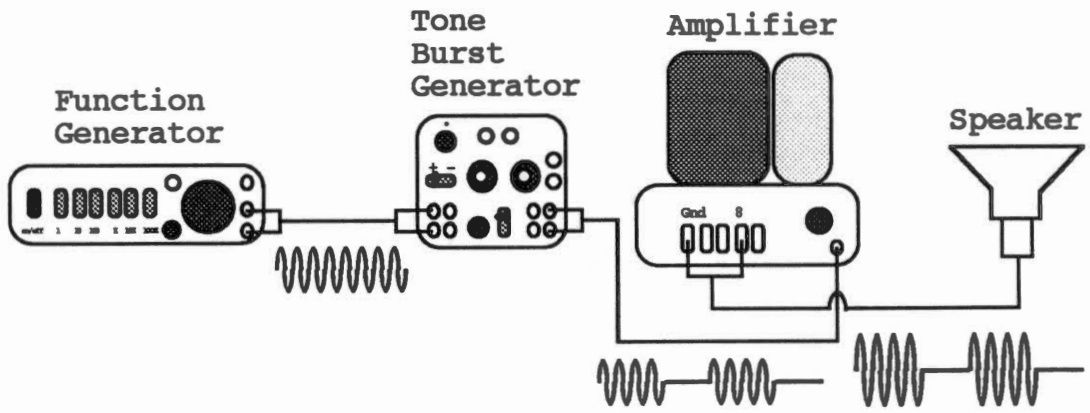

Figure 6. Schematic Diagram of Speaker System

If a continuous sinusoidal signal is used, the velocity of propagation cannot be determined. However, with a one-end (Figure 3) or both-end terminated signal the measurement of

wave propagation becomes possible. Therefore, a tone burst generator was used to allow certain wave motions to be passed through and others to be cut out (attenuate). Since the terminated signal makes it easier to determine when the signal starts, the time delay between the two signals detected by the sensors can be more easily defined.

3.2.2 Point-Source System

A pneumatic pulser designed by Dr. Lowery was constructed and tested in this study. Its schematic diagram is shown in Figure 7. As the solenoid valve opens with a sudden release of high pressure, a strong non-linear acoustical pressure wave forms in the pressure tube. In this case, higher frequency components move slower, and the wave front becomes steeper as the wave travels down along the pulser tube and forms a shock wave. When the shock wave emerges from the tube, it excites the web. The air pressure can be varied by the regulator from 0 to 60 psi. Most of the time the pressure is set at 30 psi. The accumulator, made with a 2-inch PVC schedule 40 pipe and 2 caps (stoppers), can supply enough air to pass through the solenoid valve each time it opens. The accumulator also maintains a constant pressure source and acts to damp out the pressure fluctuation in the pressure line.

Figure 8 shows the electric circuit diagram of the pulser valve controller. A DC power supply charges the capacitor to approximately 40 volts. A TTL pulser generator

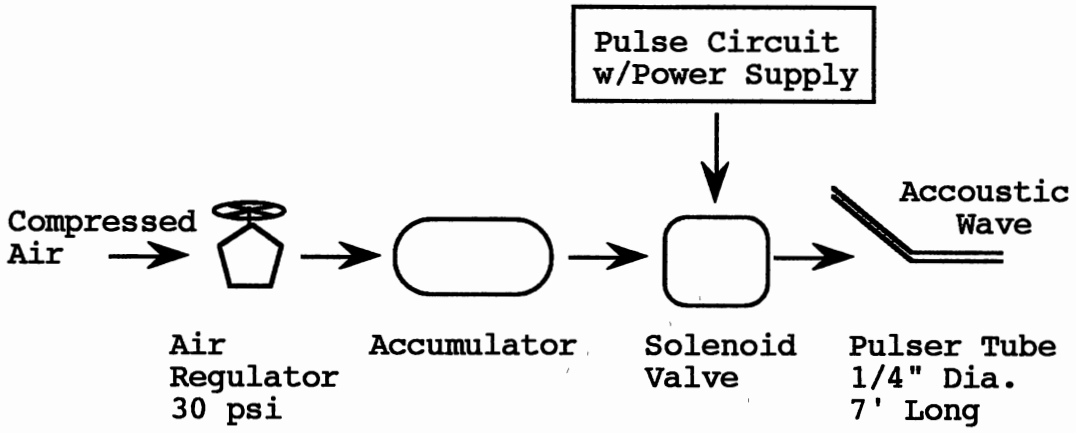

Figure 7. Schematic Diagram of Point-Source System

controls the capacitor to discharge to the valve coil. As the coil is supplied with enough energy, the armature jumps off its seat sharply and leaves the valve open. In the mean time, the DC power supply also provides five volts to a 555 timer chip which controls the frequency of valve opening and closing. Two potentiometers are used for adjusting the duration and interval between the opening of the valve. The duration of valve opening controls the width of the pulse which is about 200 microsecond. This circuit has proved to be very successful and inexpensive.

The pulser tube can be arranged in three configurations. The tube can point to the web in the normal direction; it can be flat and point to sensors along in the machine direction; or it can be set in the cross direction. These are shown in Figure 9. When the pulser tube directly points to the web, a significant air effect is observed. The results of tube

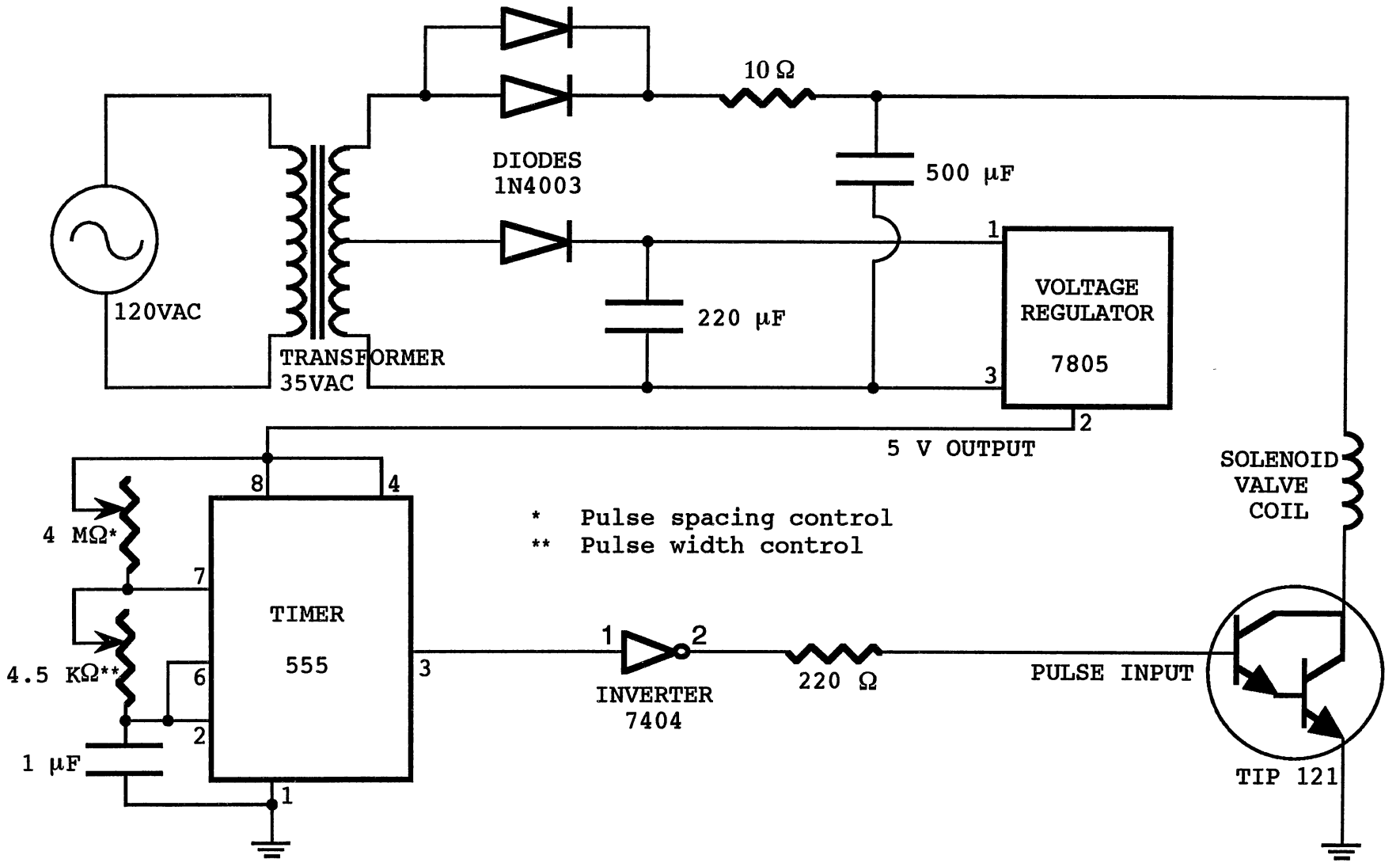

Figure 8. Circuit Diagram for Driving Solenoid Valve

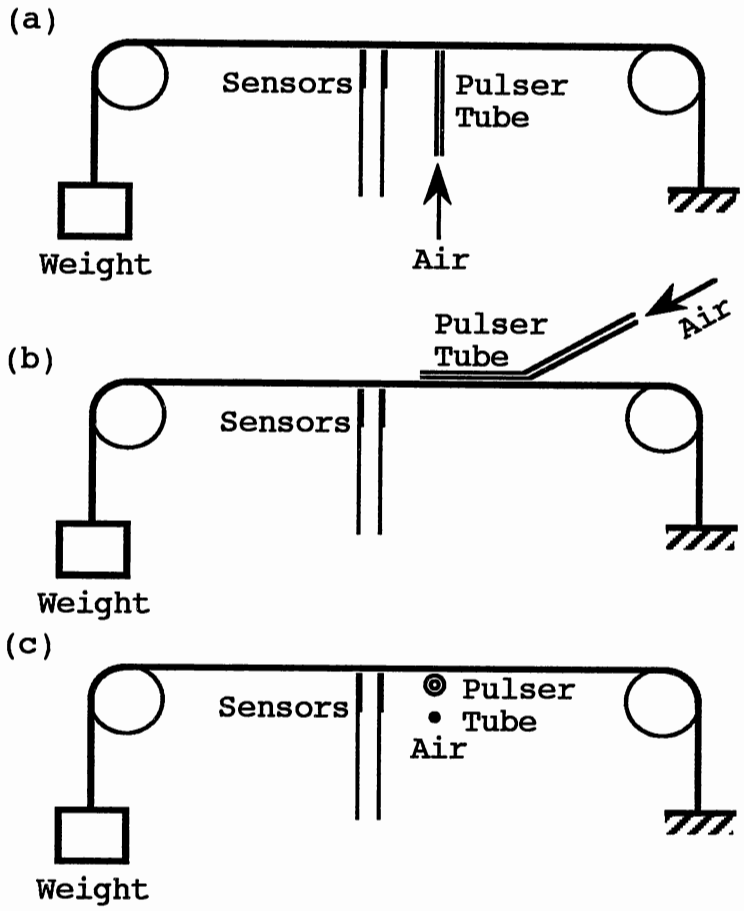

Figure 9. Orientations of Pulser Tube
(a) Normal Direction
(b) Machine Direction
(c) Cross Direction

orientation will be more fully discussed in Chapter IV.

Previous students of Dr. Lowery have examined several types of tubing and solenoid valves (26). The best pulse was produced by "Eemco" or "MAC" solenoid valves with hard wall tubing such as aluminum, copper, and polypropylene tubing. The length and diameter of the tubing were also tested for optimum size. The conclusion from their report is that a 7-

foot-long white polypropylene tubing with 1/4- or 3/16-inch-inside diameter is recommended and was used for the pressure line of this pneumatic pulser. Appendix C gives the additional testing data for Eemco solenoid valves of different orifices, coils, and springs, which were considered for use in this research.

3.3 Sensors

Several types of sensors were used in this study to detect the traveling wave which an acoustic sound burst introduces into the web. The following subsections describe them in more detail.

3.3.1 Microphones

Microphones are basically pressure measuring devices. Electrical output signals are due to mechanical movements of the thin diaphragm caused by the pressure fluctuations acting against it. As a wave travels in the web, its surrounding air pressure is also disturbed proportionally to the rate of change of the web deflection. Although this pressure fluctuation is very tiny, it still can be sensed easily by ordinary inexpensive microphones whose sensitivity is more than adequate. Microphones not only sense the pressure fluctuation caused by the web movement but also sense the sound pressure from the sound burst. Therefore, it is necessary to have a method to distinguish which wave form is caused by the web movement before analyzing the signal.

Two types of microphones have been used in this study. One type is the condenser (or capacitor) microphone. The diaphragm of this microphone acts as the moving plate of a capacitance-displacement transducer and results in an output voltage corresponding to the deflection of the plate. One of the best this type is the Bruel and Kjaer (B&K) model 4135 1/4" microphone with an integral amplifier. Its pressure-field microscope has very high sensitivity and excellent high frequency response. It worked very well in this study. The other type is an Electret microphone which is a special form of the condenser type with integral FET amplifiers. This type of microphone has self-polarizing voltage. Two makes of this type, the Radio Shack and Panasonic P9930 microphones, have been tested. Both of them work well in this study. Appendix D shows the shaker test for a Electret microphone and a OPTEK sensor.

3.3.2 OPTEK Sensors

OPTEK model OPB 125, 700, 701 sensors have been examined. They are low-priced, common reflective sensors and work equally well on most of the materials tested in this study. The OPTEK sensor consists of an infrared emitting diode and an NPN silicon phototransistor mounted side-by-side on a converging optical axis. The phototransistor responds to reflective radiation from an object within the sensor's view field. Its output signal corresponds to the object distance.

Sample static calibration curves for OPTEK model OPB 125 are attached in Appendix E, which shows output signals as a function of distance from the reflective surface. This calibration is accomplished by using 3-mil paper as a reflecting surface. The greatest sensitivity, shown by curve with positive slope (Appendix E), is seen to occur at distances of less than 0.1 inch. For most of the tests in this study, the sensor was operated in the near-field, at distances less than 0.1 inch.

Although the response of the optical sensors is nonlinear and is affected by many factors, such as rotation of the surface and changes in reflectivity, the peaks of the wave will still be sensed at the correct time. The non-linearity of the sensors will not affect the correct wave traveling speed calculation. The rise and fall times of the OPTEK's response depends on the load resistance used in the circuit. Because the maximum forward voltage is 1.7 V with a current of 50 mA for the input diode, a 1000 Ω load resistor is used in the circuit. Based on the data sheet, the frequency response of this circuit is probably around 6 KHz.

3.3.3 Laser Vibrometer

A laser vibrometer permits vibration measurements without any influence on the vibrating surface. It can measure the velocity of a vibrating surface based on the interferometric principle. This instrument functions by emitting a laser beam onto a moving object and detecting the

Doppler frequency shift of the back-scattered beam caused by the movement. Appendix F gives the schematic and block diagrams of the Polytec OFV 2600/OFV 3500 laser vibrometer.

A low power (CW 2mW) He-Ne laser beam is divided into two equal-intensity, parallel beams by the beam splitter. One beam passes through the Bragg cell. The other beam directly focuses on the vibrating object, reflects back, and mixes with a reference beam. The reflected beam is collected by the photodetector, which contains velocity information in terms of a Doppler shift. It then goes through a mixing process in a mixer, demodulation in the velocity decoder unit, and filtering process in low-pass output filter unit. It finally appears an voltage output signal. The output voltage is proportional to the instantaneous object velocity. The operating frequency range for this laser vibrometer is from 0.001 to 100 KHz. The sensitivity is based on the selection of three velocity decoder range settings.

3.4 Testing Materials

Various types of webs have been tested to verify the point-source process. The webs tested include Kodak film paper, single-layer tissue paper, 3-mil white paper, 3M recording medium, Mylar tape, polypropylene, adhesive tape, and Mead 80 LB. Signature Dull. Although all the materials listed in Table I were tested in this study, most of the experiments were performed on either 3M recording medium or Mead 80 LB. Signature Dull.

Table I

PROPERTIES OF WEBS

Type of Web	Width (in)	Thickness (m)	Density (Kg/m^2)	Young's Modulus (N/m^2)
Kodak Paper	2 3/4		0.2523926	
Single Layer Tissue paper	6 1/10		0.016679	nil
3-mil Paper	6		0.055266	
3M Recording Medium	5 3/8	7.94e-5	0.115398	3.45e9
Mylar tape	5/8		0.160458	
Polypropylene	4 1/4		0.021789	
Adhesive Tape	5		0.06168	
Mead 80 LB.* Signature Dull	6	9.84e-5	0.1213	7.32e9

*The data are provided by Mead Company.

3.4 Stiffness Measurement Experimental Setup

If a stiff web is short enough, it acts like a beam. As long as the web is slender enough (having a 10 to 1 ratio of length to width) the rotary inertia term can be omitted from the beam equation. Figure 10 shows the setup for measuring the stiffness. One OPTEK sensor is placed near the clamped end. By tipping the free end, the sensor and the

oscilloscope can detect and record, respectively, web motion. Then, measurements of amplitudes and the time between two successive peaks, will determine the damping period. By applying the equation of motion for a cantilever beam, stiffness (EI) of a web can be determined.

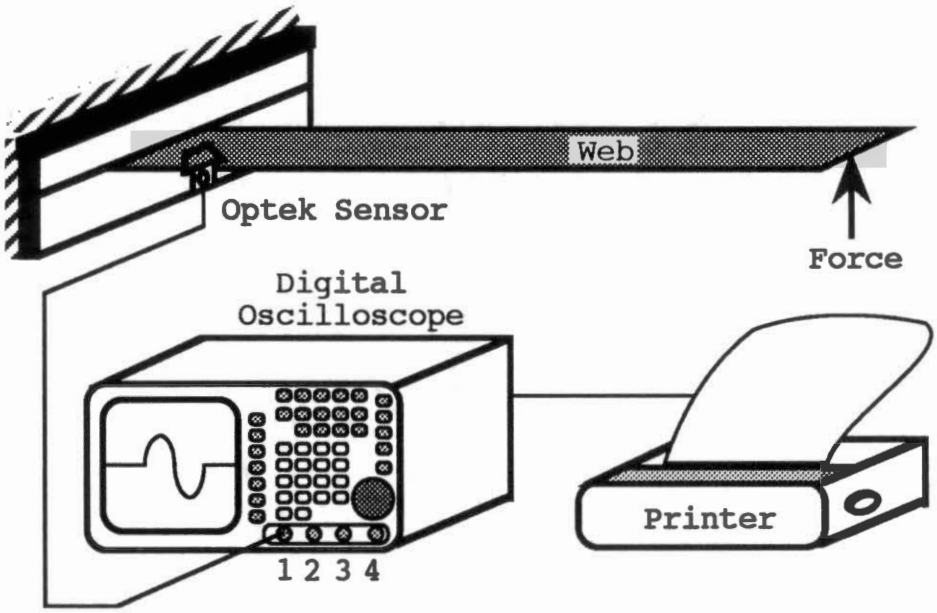

Figure 10. Setup for Measuring Stiffness

CHAPTER IV

RESULTS & DISCUSSIONS

The experimental and theoretical results are addressed in this chapter. The analytical solution of the tensioned-plate model with air-loading is obtained and presented in section 4.1. With the speaker system, all the models have been examined. Their resulting predicted tensions and velocities are discussed in section 4.2. The effect of air loading is included in section 4.3. Since the stiffness is required in some of the models, section 4.4 has the Young's modulus from the experimental results. Then, section 4.5 addresses how the pulser tube orientation, air source pressure, distance, tension, and materials effect the point-source process. In section 4.6, forerunners are exemplified by a single pulse wave traveling a certain distance. Section 4.7 shows the experimental results by pneumatic and mechanical excitations. Finally, an attempt to compare the experimental and numerical results is given in section 4.8.

4.1 Tensioned-Plate Model with Air-Loading

A pure membrane is just an ideal case. In reality, a web is always in between a membrane and a plate. Based on

the literature, the general equation describing the motion of a thin web would be the membrane model with air loading because most of the time the error percentage from stiffness is not significant. Only when thicker material is dealt with, does the model have to include the stiffness term as a restoring force. Of course, tension still plays an important role in the membrane model. By incorporating the air loading term with the stiff string or tensioned-beam model, the equation of motion is then modified as

$$T \frac{\partial^2 \eta}{\partial x^2} - EI \frac{\partial^4 \eta}{\partial x^4} = (\sigma_1 + \frac{2\rho}{\sqrt{K^2-k^2}} b) \frac{\partial^2 \eta}{\partial t^2}$$

Solving for tension in terms of phase velocity gives (refer to Appendix G)

$$T = (\sigma_1 + \frac{2\rho}{\sqrt{K^2-k^2}} b) V_{ph}^2 - EI \frac{\omega^2}{V_{ph}^2}$$

or vice versa,

$$V_{ph}^2 = \left(\frac{T + \left(T^2 + 4(\sigma_1 + \frac{2\rho}{\sqrt{K^2-k^2}} b) EI\omega^2 \right)^{1/2}}{2(\sigma_1 + \frac{2\rho}{\sqrt{K^2-k^2}} b)} \right)^{1/2}$$

The above equation shows that the phase velocity depends not only on frequency but also on tension, density, thickness, width, and stiffness of a web. Since a single pulse can be resolved into a series of frequency components, it will experience dispersion. In other words, the shape of the pulse keeps changing along its traveling path. Absorption is not considered in any of the models. In the ideal case, tension is obtainable by calculation, as long as phase

velocity can be determined and the web's properties are available. Then, no calibration curves are needed.

4.2 Speaker with Tone Burst System

It is much easier to validate the tensioned-plate model with air-loading by using a single-frequency wave. The speaker with a tone burst system can provide a terminated wave which helps to determine a phase velocity in a web. Tests were run on the Mead web cut to 6 inches width to fit the setup. The operating tension ranges from 85 to 202 N/m (0.5 to 1.2 pli) and frequency ranges from 0.3 to 1 KHz. Due to higher frequency waves exciting the web too strongly, the speaker does not only generate a traveling wave into the web but also vibrates the whole web span. Therefore, the OPTEK sensor has trouble with not getting good signals because of its sensitivity to the gap between the web and the OPTEK sensor itself. It picks up both motions of the traveling wave and vibrating web. After the experiment was performed, the laser vibrometer became available. The motion of the vibrating web span did not have much effect on the detected signal of the laser vibrometer. Frequency can be run up to 3 KHz.

Appendix H lists the experimental and predicted tensions and Figure 11 shows the results. The predicted tensions are based on string, membrane with air-loading, tensioned beam, and tensioned plate with air-loading wave equations. Each of the graphs in Figure 11 presents the predicted tensions with

(a)

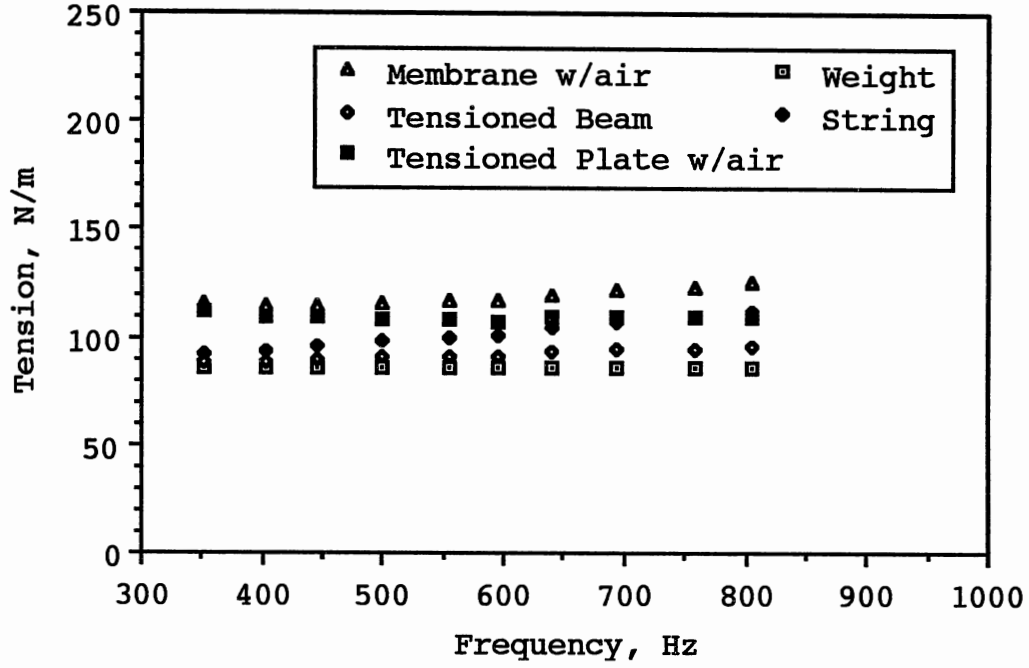

(b)

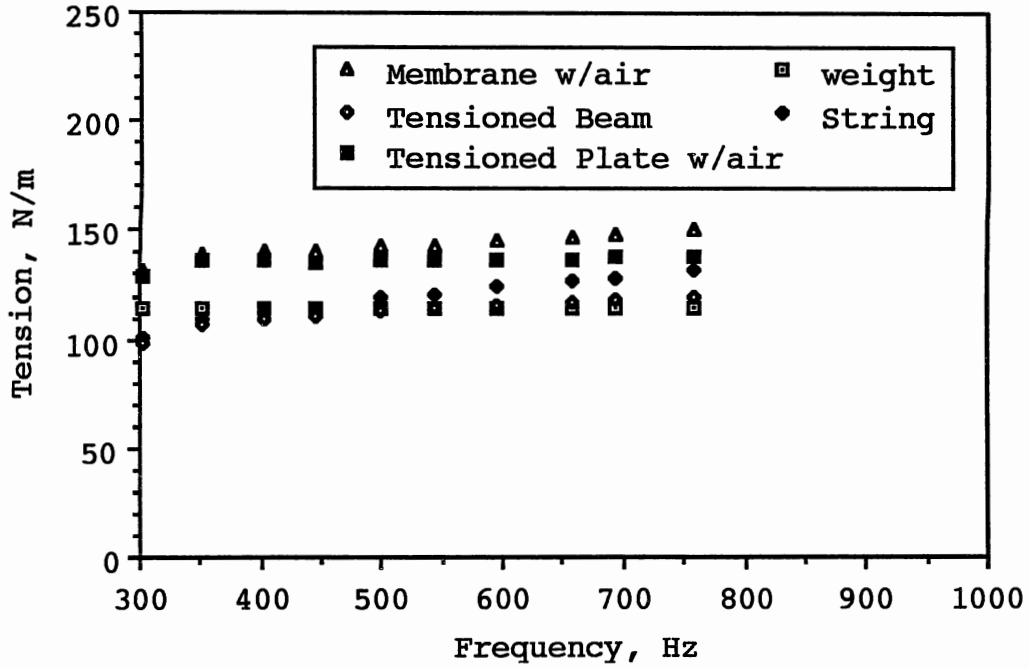

Figure 11. Predicted Tensions by Different Models with Various Frequencies at (a) 85 N/m (b) 114 N/m (c) 144 N/m (d) 173 N/m (e) 202 N/m

(c)

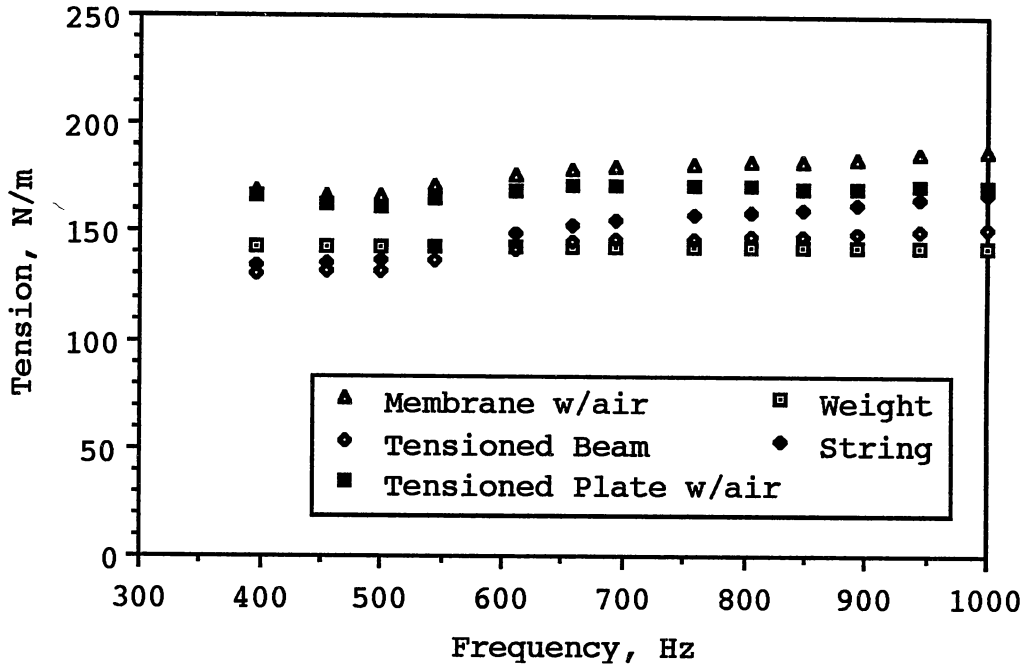

(d)

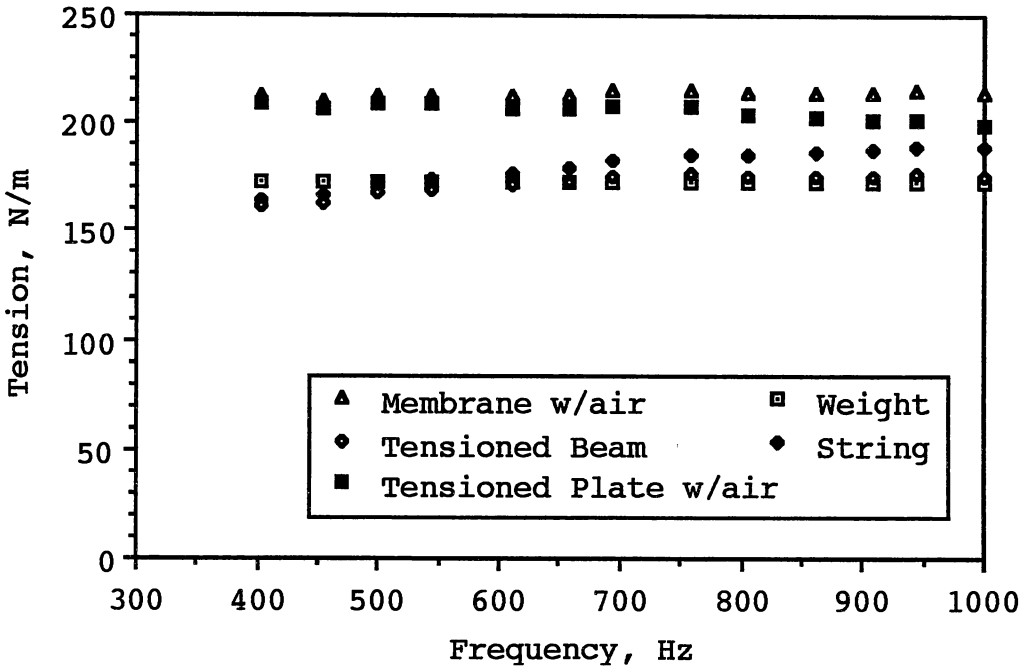

Figure 11. "Continued"

(e)

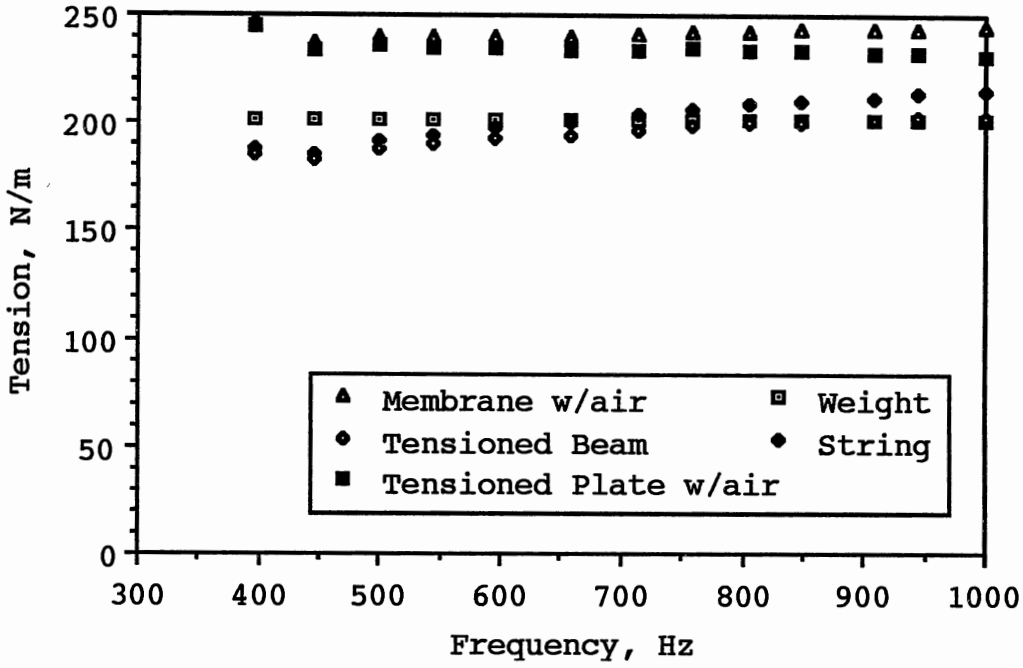

Figure 11. "Continued"

varying frequencies at fixed tension indicated by the symbol of weight. All the models but one show the increasing predicted tension with increasing frequency. The tensioned-plate model is the only one which predicts the correct tendency. However, the tensioned-beam model predicts tension values which are closer to the dead weight values. The air-loading term makes the predicted tension too high for both membrane and tensioned-plate models. For the tensioned-plate model, the highest error percentage of the predicted tension is 28% in the 85 N/m (0.49 pli) case. A value of 85 N/m is considered fairly low tension. The rest of the error percentages are 19, 18, 19, and 16%.

A close examination of the two models for obtaining the air-loading term shows that web thickness is not so small that air load can be assumed to be twice the air pressure wave at $\eta=0$. Based on Merilainen's results (18), the predicted velocities are lower than measured ones at frequencies less than 2 KHz. Therefore, instead of tensions, the velocities were predicted as shown in Figure 12 (see Figure 40 in Appendix I for a broader frequency range), using the same set of data. As expected, the predicted velocities are lower than the measured ones, and the tendencies of the predicted and measured velocities are in accord. The error percentages of the predicted velocities are around 10% for the tensioned-plate model. If the velocity were targeted for the prediction, the model could provide very satisfactory results, especially at higher frequencies (18). However, the tension is the target. The overall error percentage should be about 20% depending on the operating tension.

4.3 Effect of Air-Loading

Tests have been run to examine the effect of air loading. A Plexiglas plate was set up above the testing web. By attaching the Plexiglas plate to a vertical traverse mechanism, the distance between the plate and the testing web can be varied consistently (inducing varying amounts of additional air load). This time, 3M recording medium was used under the tension of 193 N/m (1.1 pli). To avoid the complexity of determining multi-frequency wave traveling

(a)

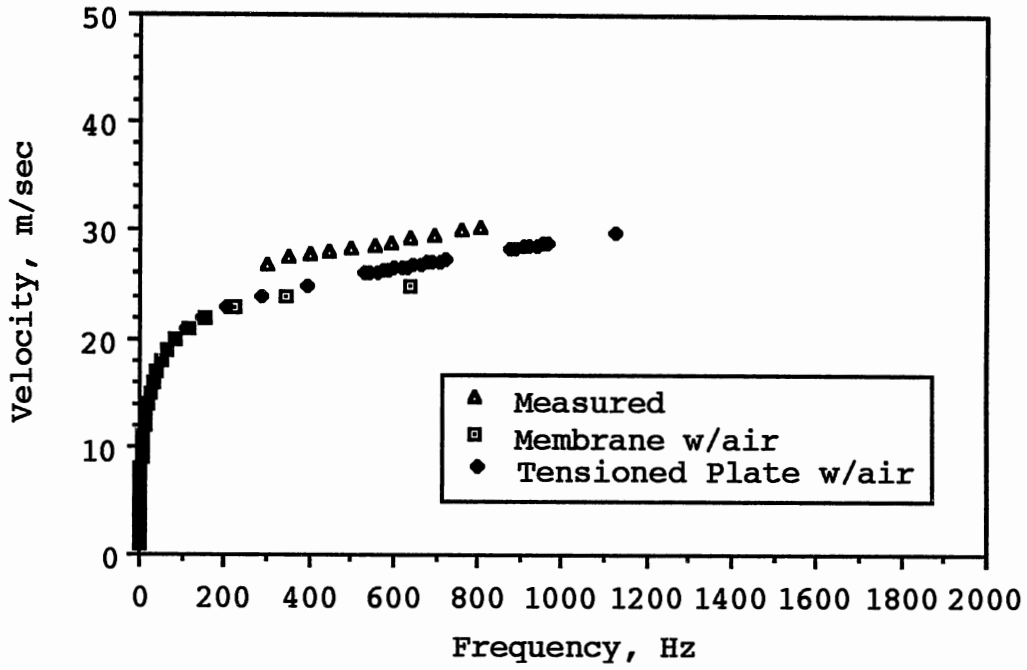

(b)

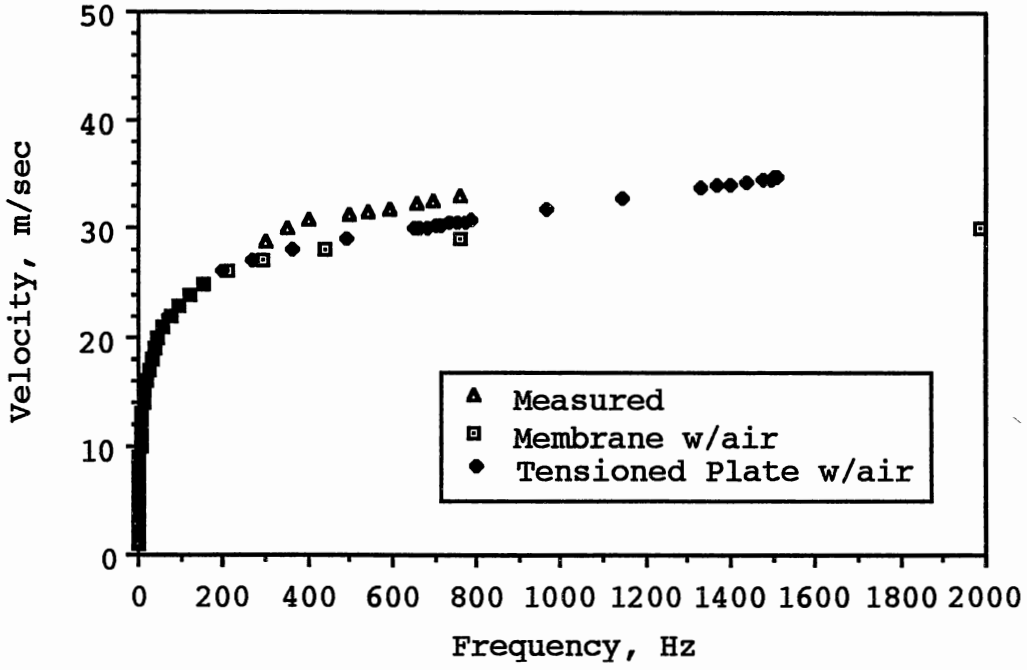

Figure 12. Predicted Velocity by Different Models with Various Frequencies at (a) 85 N/m (b) 114 N/m (c) 144 N/m (d) 173 N/m (e) 202 N/m

(c)

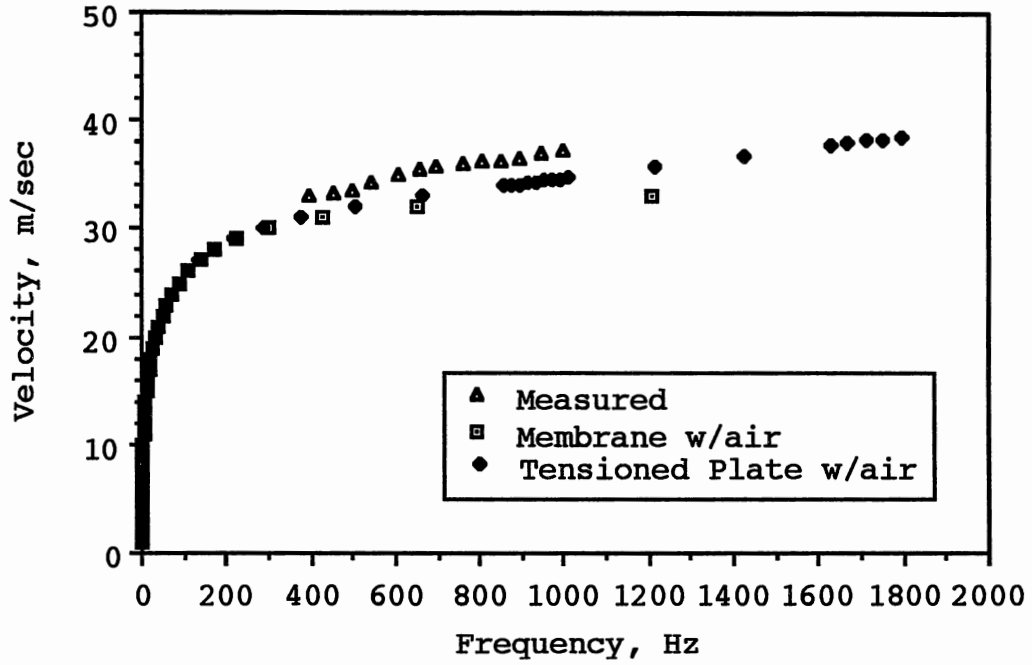

(d)

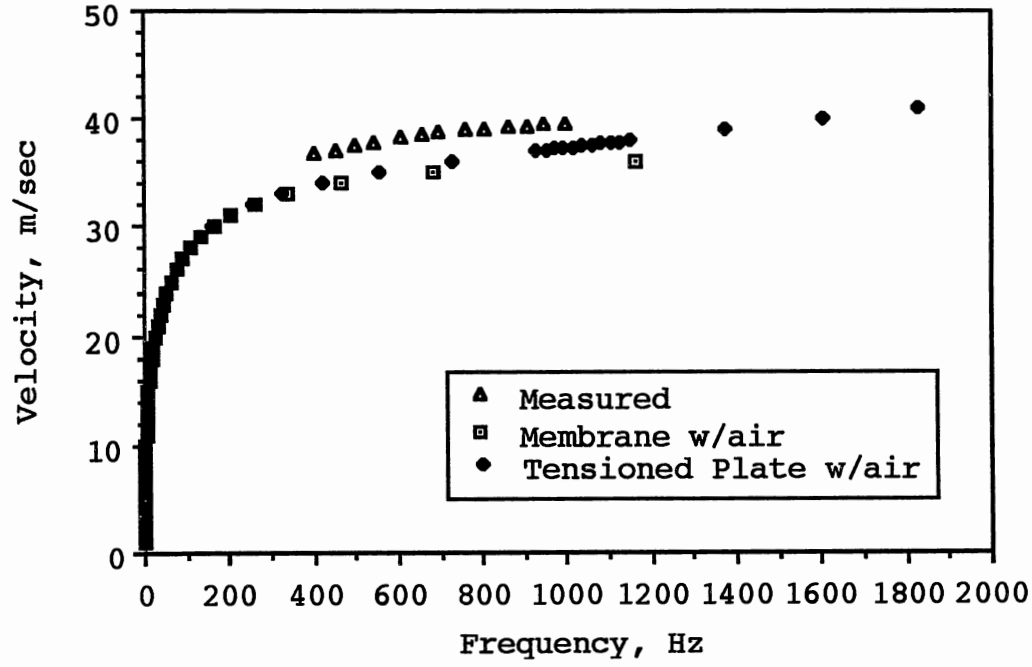

Figure 12. "Continued"

(e)

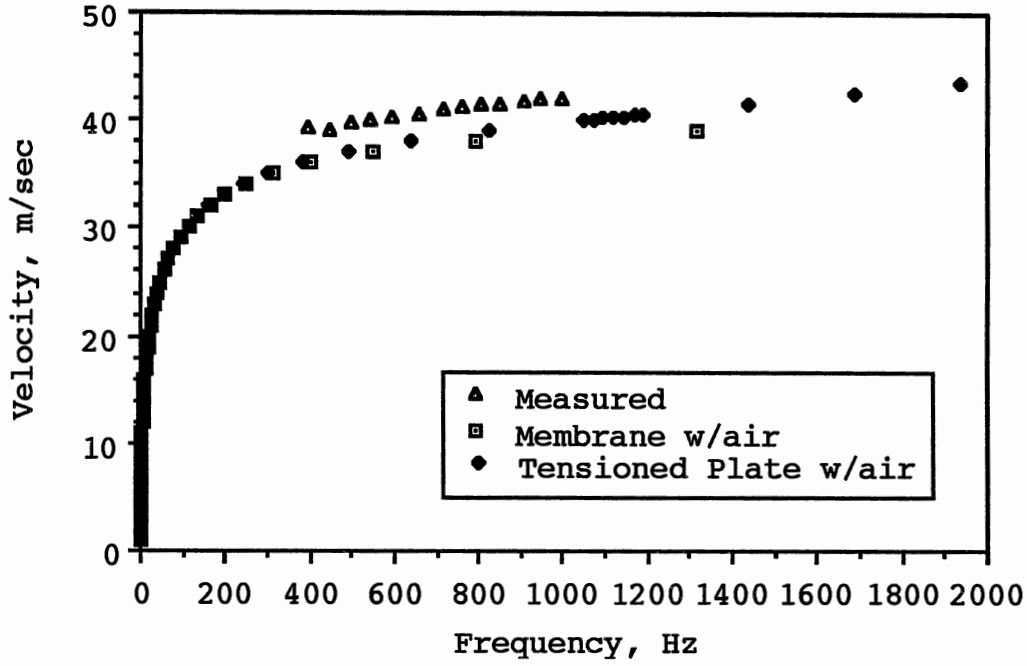

Figure 12. "Continued"

velocity, the speaker system setup was selected and operated at 2000 Hz. The two OPTEK sensors used are 0.1035 m (4.075 in) apart to track the time of flight. The result is shown in Figure 13 and the corresponding experimental data are listed in Appendix J. The distance between the web and the Plexiglas plate varies from $8.9*10^{-4}$ m (0.035 in) to where the traveling velocity in the web approaches a constant. As the distance increases, the velocity also increases. The velocity starts from 42.42 m/sec and approaches to 45.4 m/sec at the distance of 0.0127 m apart. Further increment of the distance does not change the wave velocity because the added air-loading mass stays constant. Based on the data, the

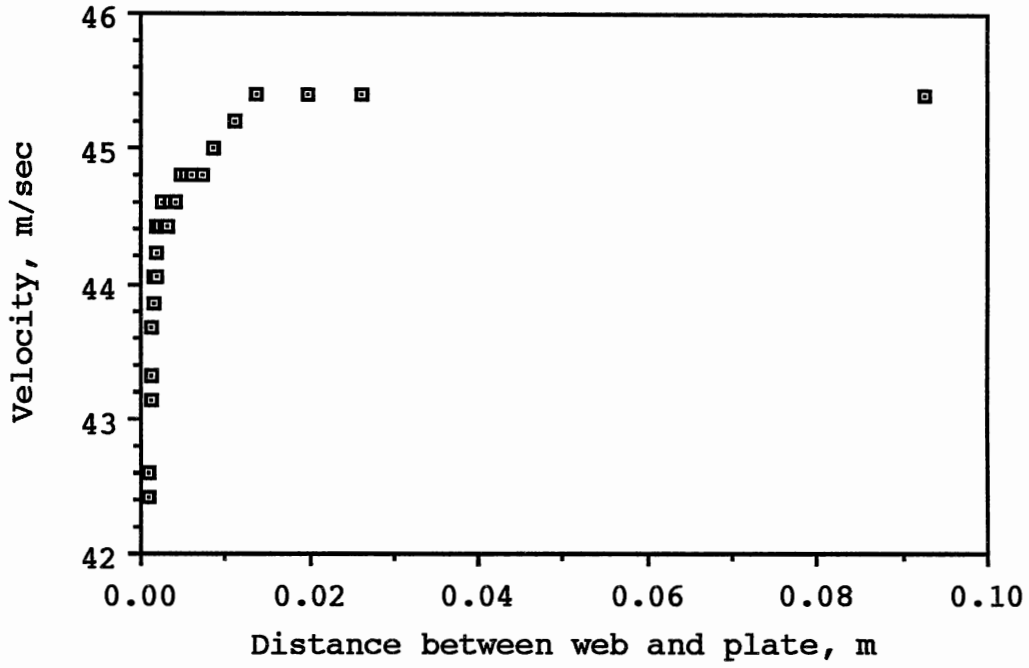

Figure 13. Air Loading Effect

difference of wave velocities (above) due to the additional air-loading effect is about 7% in this case.

4.4 Stiffness

For a thick web, stiffness is a required datum. Since the Young's modulus of the 3M recording medium was not available, a test was run to obtain it. Due to not knowing the accuracy of the Young's modulus measurement that the stiffness experimental setup provides, tests on the Mead web were performed first because of its known properties. The selected test specimens were 1 cm wide and 10 cm long. The successive amplitudes and the damping frequency of the

vibration are measured. Appendix K gives a sample calculation. The test results for the five specimens of the Mead web are 7.14e9, 7.21e9, 6.78e9, 7.78e9, and 8.91e9 for five runs. They are very consistent and their average is 7.56e9 N/m^2. Compared to 7.32e9 N/m^2, the measurement provided by the Mead Company, the agreement is quite satisfactory. Then, using the same setup and procedures for the 3M recording medium, the Young's modulus is found to be 3.45e9 N/m^2. Additional tests on the recording medium are required to verify the precision of the Young's modulus of the 3M recording medium.

4.5 Point-Source Process

Since the pulse wave induced into the web is not a single frequency wave, the measured traveling wave velocity in the web is signal velocity. As mentioned in Chapter II, signal velocity is group velocity if absorption is not strong. Therefore, the velocity measured based on oscilloscope traces or the cross-correlation method is not phase velocity. Only a sinusoidal wave can travel without changing its shape, even in dispersive media, and the measured traveling velocity is indeed phase velocity. To be able to use any models, phase velocity is required. Chapter II states that the group velocity is twice its phase velocity for the mean frequency in the group for both the beam and plate models. This raises another question: what is the mean frequency? Is the mean frequency the same as characteristic

frequency? Further study about a single-frequency system might help gain more knowledge to explain it. The point-source system is such a complex process that many factors need to be examined and will be addressed one by one in the following subsections.

4.5.1 Pulser Tube Orientation

Bradley (28) states in her master's thesis that "The signals became shorter in duration and had a higher peak voltage with increasing tension." Based on Bradley's finding, further investigation of this phenomenon was continued. A 3-mil-thick paper was tested with a 30 psi air source. The Electret microphone was used to detect wave signals and set 4 inches apart from the pulser tube.

Two orientations of the pulser tube were employed. First, the air from the pulser tube was directly impinged into the paper (the normal direction). The range of tension was from 173 to 465 N/m (0.99 to 2.65 pli). Recorded wave forms are shown in Figure 14, and indeed, the results are just as Bradley states in her thesis. In addition, the amplitude changes very little at high tensions. Second, the same set-up and parameters were used except for changing the orientation of the pulser tube to the cross direction. Based on the same set of tensions, Figure 15 shows the different wave forms. The amplitudes and the durations (shapes) of the second set of wave forms do not change as tension increases.

These two sets of records turn out totally different.

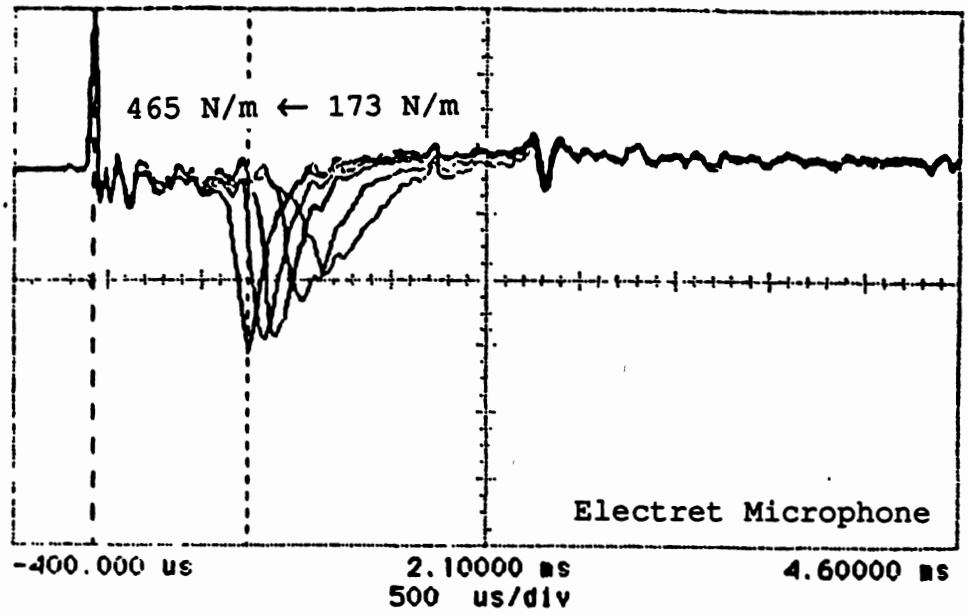

Figure 14. Wave's Responses to Pulser Tube in Normal Direction

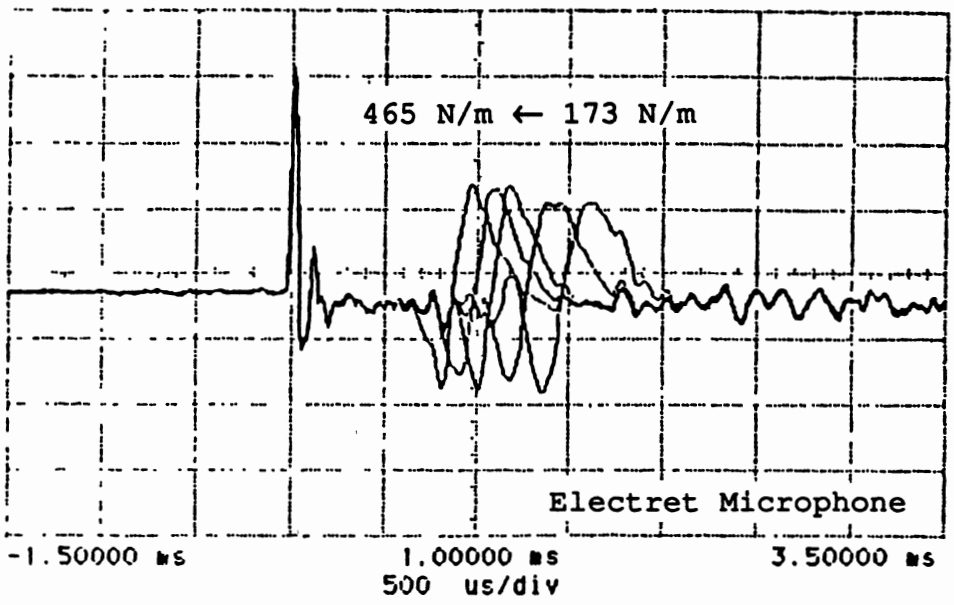

Figure 15. Wave's Responses to Pulser Tube in Cross Direction

The only thing that makes is different in the experimental setup is the orientations of the pulser tube. Therefore, the phenomenon described in Bradley's thesis is not simply due to the tension of the web. This phenomenon must be, therefore, due to the interaction between air dynamics and a tensioned web. It might be possible to develop a method to measure tension with normal pulser tube direction based on the changing height of wave forms. However, there are many other factors besides tension to be considered, such as, air pressure, tubing length and diameter, distance between the web and the pulser tube, and material of the web. The width of web might even have some effect.

Additional tests were run with various incident angles between the pulser tube and the web. The 3M recording medium was used at a tension of 193 N/m (1.1 pli). The pulser tube was 8 inches apart from the sensors -- a B&K microphone and an OPTEK 701. The incident angle was varied from 0° (the pulser tube was parallel to the web, i.e. the machine direction) to 90° (the pulser tube pointed downward to the web, i.e. the normal direction) in 5° or 10° increments. The distance between the edge of the tube and the web was 1/8 inch.

As indicated by the oscilloscope traces shown in Figure 16, the main signal shifts downstream as the angle increases. The front part of the waves, forerunners, keep increasing in amplitudes and then merge into the main signal. These forerunners arrive at the sensors well before the main

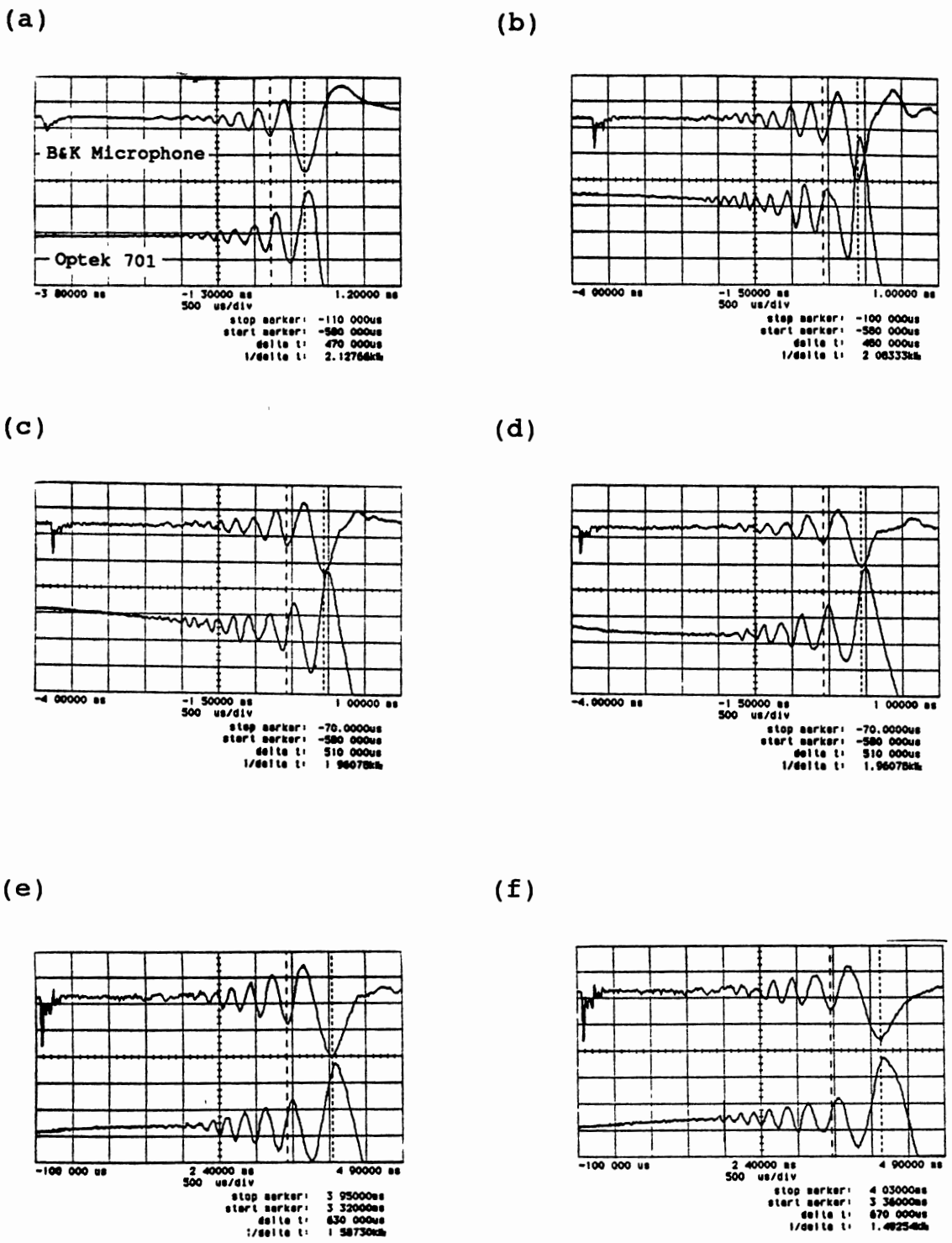

Figure 16. Wave's Responses to Various Angle between Pulser Tube and Web (a) 0° (b) 30° (c) 40° (d) 50° (e) 60° (f) 70° (g) 80° (h) 90°

(g) (h)

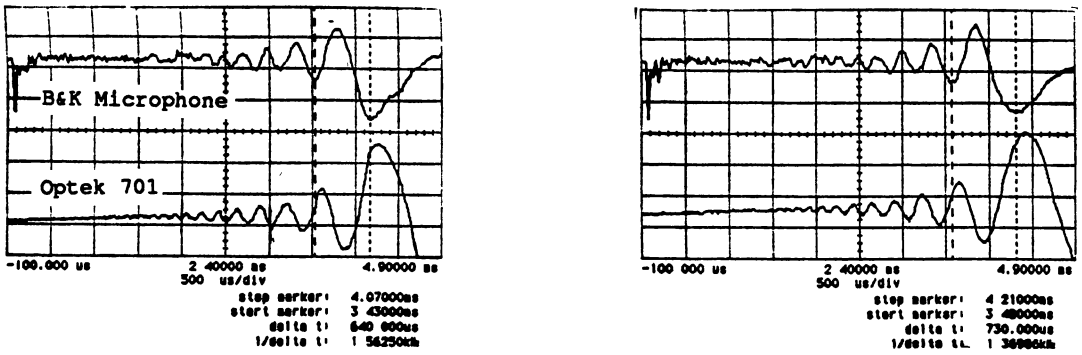

Figure 16. "Continued"

signals and their shapes are predictable. The effect has been seen in several types of webs, and has been detected both by the acoustical and optical detectors. The width (duration) of the main signal increases with the angle of the pulser tube, which agrees with the result in the previous paragraph. As the wider pulse is induced into the web, it travels slower because it contains more lower frequency components. Therefore, this explains why the main peaks shift downstream.

4.5.2 Pressure Variation of Air Source

As the pressure of the air source changes, the intensities of generated sound waves in both the air and the web also change accordingly. A higher pressure source gives higher amplitudes of sound waves in both of them (Figure 17). The pressure of the air source was ranged from 25 to 40 psi

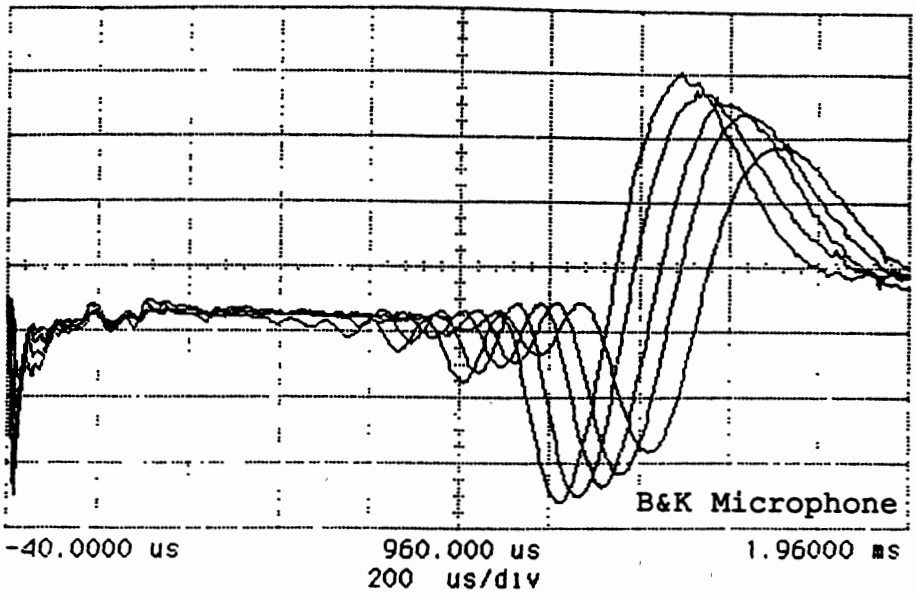

Figure 17. Wave's Responses to Various Air Pressure Source from 25 to 40 psi

in 5 psi increments, with an additional increment at 27.5 psi. A quarter-inch B&K microphone was used to detect the sound waves. It was 3 5/8 inches apart from the end of the pulser tube in the machine direction. The tension was set to be constant at 193 N/m for the 3M recording medium. The amplitudes of sound waves, which were generated from the different pressures, did not vary linearly with pressure. The widths or characteristic frequencies of those waves are very close to each other. However, the higher amplitude wave in the web travels faster than the lower amplitude one.

4.5.3 Various Distances between Pulser Tube and Sensor

It is very interesting to see how the shape of a wave changes as the wave travels along a web. Tests were run on the 3-mil paper at tension 202 N/m (1.15 pli). The distance between the pulser tube and the B&K microphone ranges from 2 to 20 inches with 2-inch increments. With the pulser tube in the machine direction, Figure 18 shows part of the experimental results. Initially, the wave in the web has a very sharp peak. As the wave travels farther, the peak begins rounding up and the forerunner part of the wave seems to be getting longer, especially for those detected at 12 inches. In all these traces, the wave amplitude does not attenuate much. Therefore, absorption is not as important as expected.

4.5.4 Various Distances between Pulser Tube and Web

Figure 19 shows the corresponding waves produced by varying the distance (gap) between the pulser tube and a web. In this experiment, the adhesive tape web was used at 242 N/m (1.4 pli) tension. The distance is varied from 0 to 0.5 inches in 0.125 inch increments. The amplitude of the induced wave is increased when the pulser tube approaches the web.

The Electret microphone was mainly used. Only in the

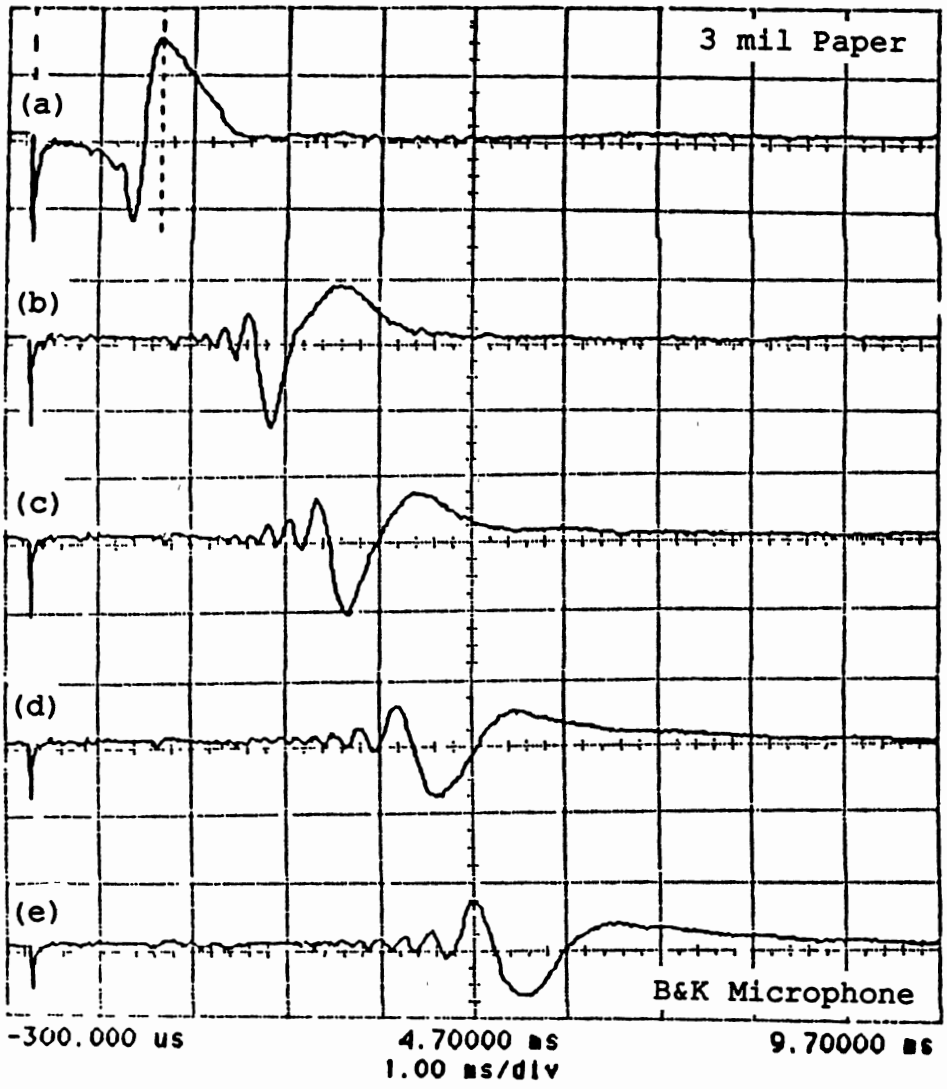

Figure 18. Wave's Responses to Various Distance between Pulser Tube and Sensor
(a) 4 inches (b) 8 inches
(c) 10 inches (d) 12 inches
(e) 14 inches

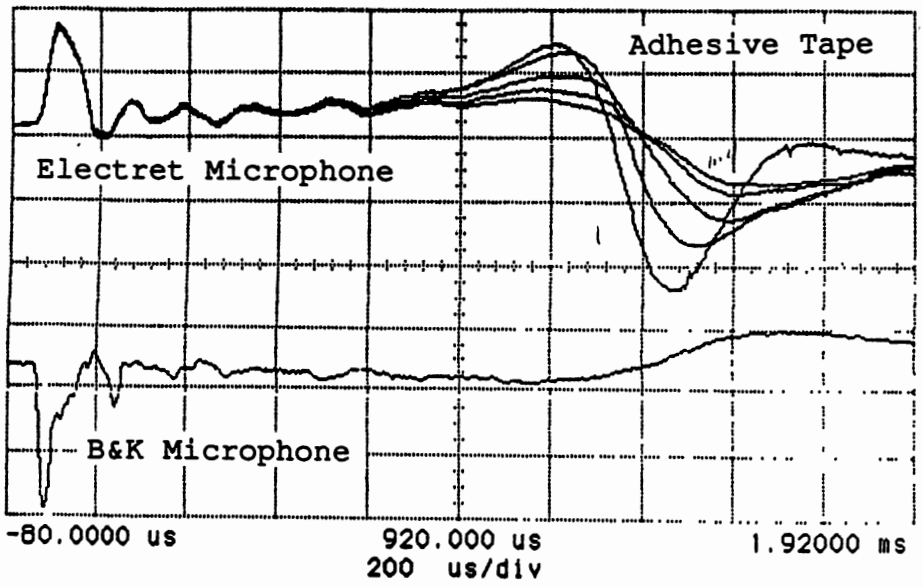

Figure 19. Wave's Responses to Various Distance between Pulser Tube and Web from 0 to 1/2 inch with 1/8-inch Increments

0.5-inch case, is the signal of the B&K microphone also shown in this figure. Both microphones show no difference when providing the main signal but they have opposite polarity. The difference between these two oscilloscope traces is that the one detected by the B&K microphone has much better high frequency response and can provide better signal output.

4.5.5 Tension Variation

Wave velocity depends on the tension in the web, and waves travels faster in a web with higher tension. Our experimental results show no exceptions in Figure 20. The applied tension ranges from 225 to 421 N/m (1.3 to 2.4 pli). Our principal concern here are the forerunners. It seems

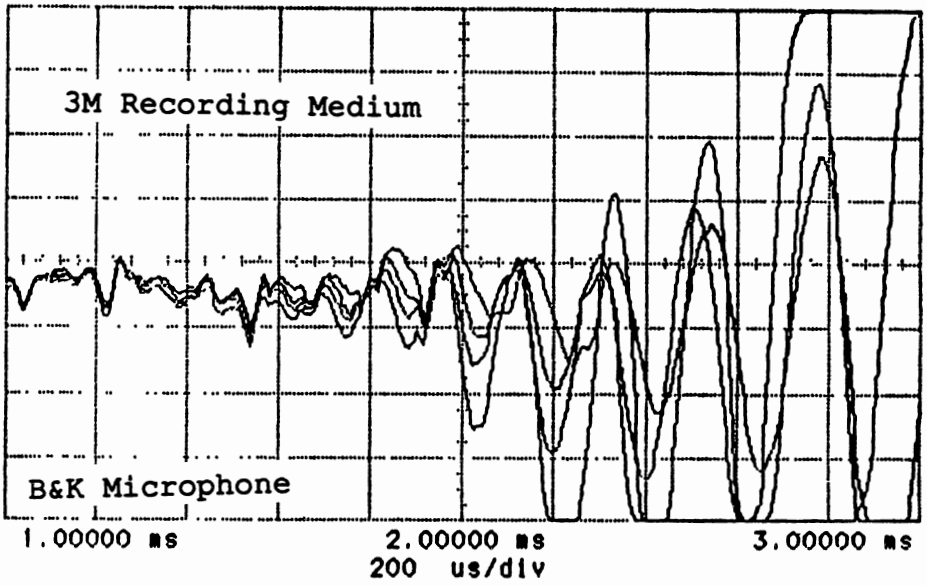

Figure 20. Wave's Response to Various Tensions from 225 to 421 N/m^2 with 65.2 N/m^2 Increments

that the forerunners start at the same place even with different tensions. However, the forerunners in webs of higher tension build up faster than those in webs of lower tension. This seems logical because the forerunners eventually join onto the main signal which has a velocity that depends on tension.

4.5.6 Material Testing

Tests were run to verify what type of webs the point-source system would work with. Products submitted by sponsors and tested included polypropylene, Kodak photographic paper, single layer tissue paper, 3M recording

medium, Mylar tape, and adhesive tape. The preliminary tests pointed toward being able to use the pulse method for almost any type of web material.

The response for the polypropylene to the point-source process in Figure 21 shows very sharp waves. The Electret microphone gives very clear output signals but the OPTEK sensor does not. As tension increases, the corresponding wave also travels faster and gets narrower.

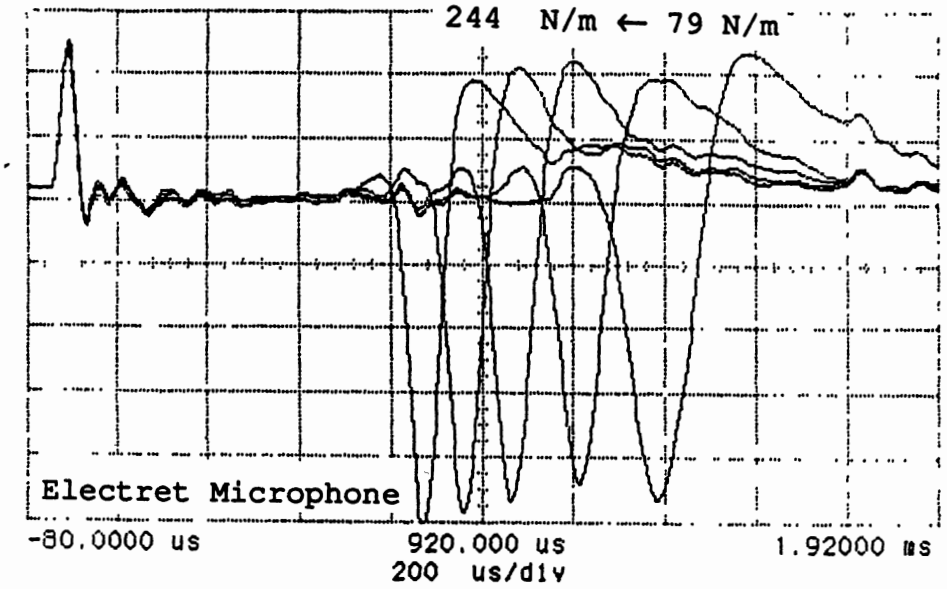

Figure 21. Pulse Waves in Polypropylene with Tensions from 79 to 244 N/m^2 with 41 N/m^2 Increments

The Kodak photographic paper did not respond well when the orientation of the pulser tube was in the cross

direction. Therefore, switching to the machine direction was necessary. Figure 22 shows one example of testing results for the Kodak photographic paper. Higher tension could be applied to the Kodak paper because it is much thicker and heavier than the other webs. Forerunners are recognizable. Both acoustic and optical sensors can be used to detect the signals.

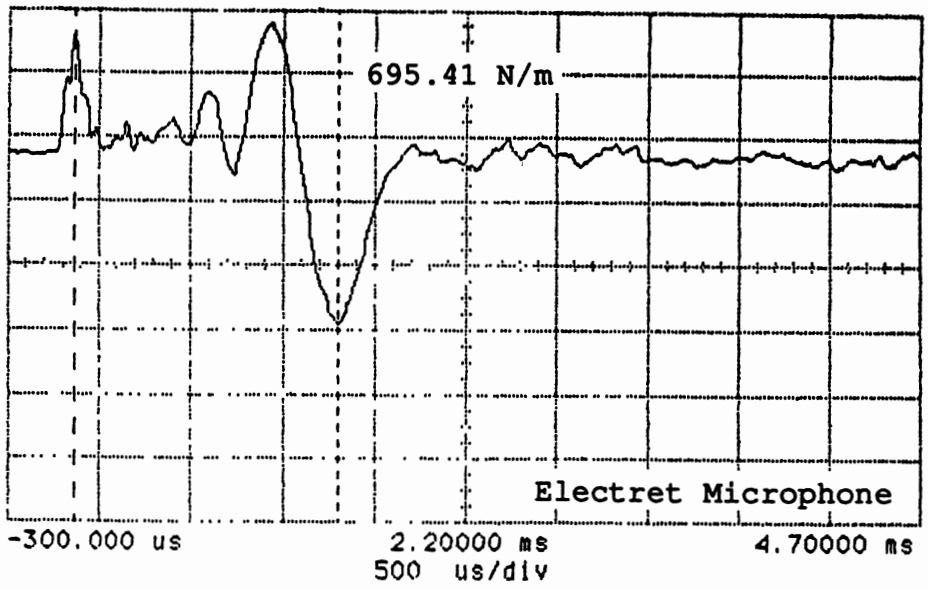

Figure 22. Pulse Wave in Kodak Paper

Rough tests for tissue paper were also run as shown in Figure 23. Since the pulser tube was placed in the machine direction, air did not blow into the tissue paper directly. Even with a 30 psi air pressure source, the system generated

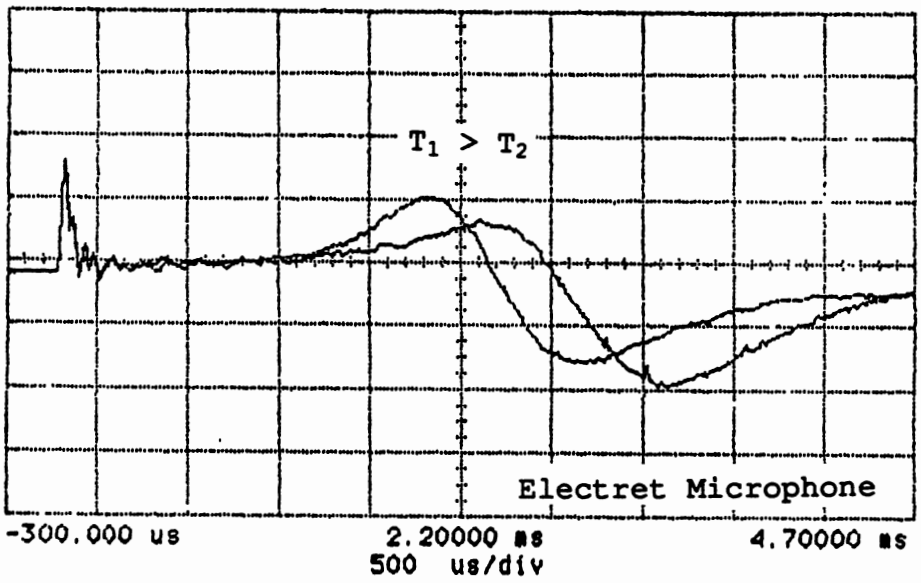

Figure 23. Pulse Waves in Single-Layer Tissue Paper at Different Tensions

signals into the tissue paper without breaking or damaging it. The waves show no trace of forerunners.

Figure 24 shows very clear forerunners in the 3M recording medium. OPTEK sensors and B&K microphones can react quickly enough to detect the forerunners but Electret microphone can not. Even so, the Electret microphone is still good enough to pick up the trend of the main signals. Forerunners are more evident in the machine direction than in the cross direction.

The adhesive tape has a glue coating layer. It is thicker than the polypropylene. The oscilloscope trace showed that the shape of the wave was changing all the time. However, the positive or the negative peak remained at the

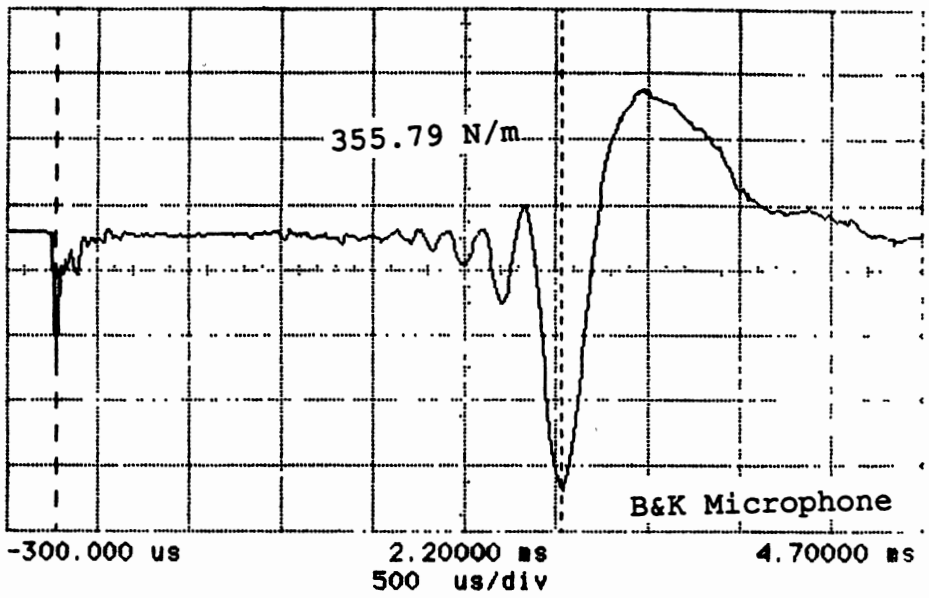

Figure 24. Pulse Wave in 3M Recording Medium

same location for each pulse. Figure 25 shows a typical output signal from the adhesive tape.

The cross and machine directions were tested for the Mylar tape. However, the signal produced from the machine direction is better than that from the cross direction. After the signal arrived, a big hump also arrived as shown in Figure 26. This was only seen in the machine direction. The reason might be that the Mylar tape is too narrow (only 5/8 inch) and the air flow has some effect upon it. One other thing worth mentioning is that the amplitude of the big hump is higher than that of the signal.

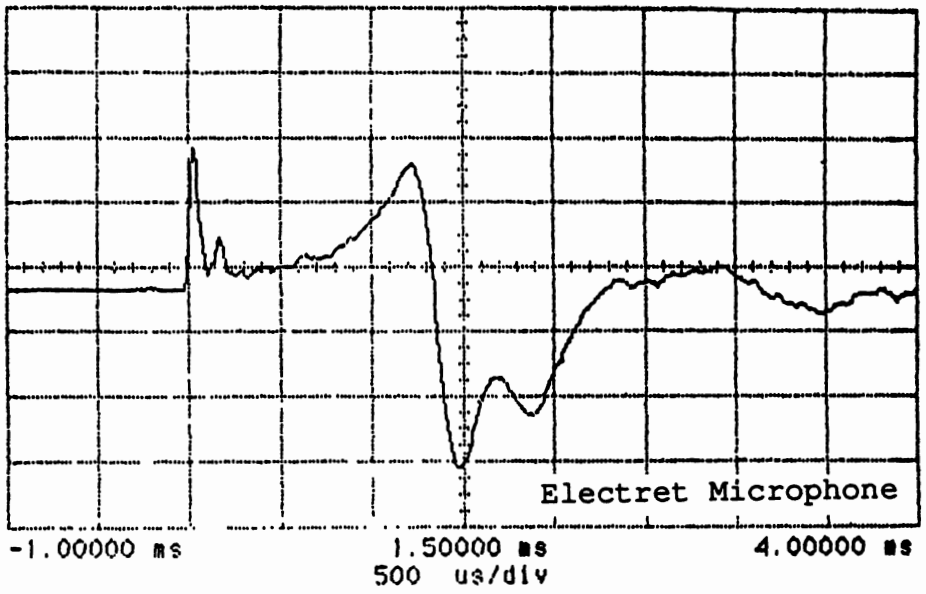

Figure 25. Pulse Wave in Adhesive Tape

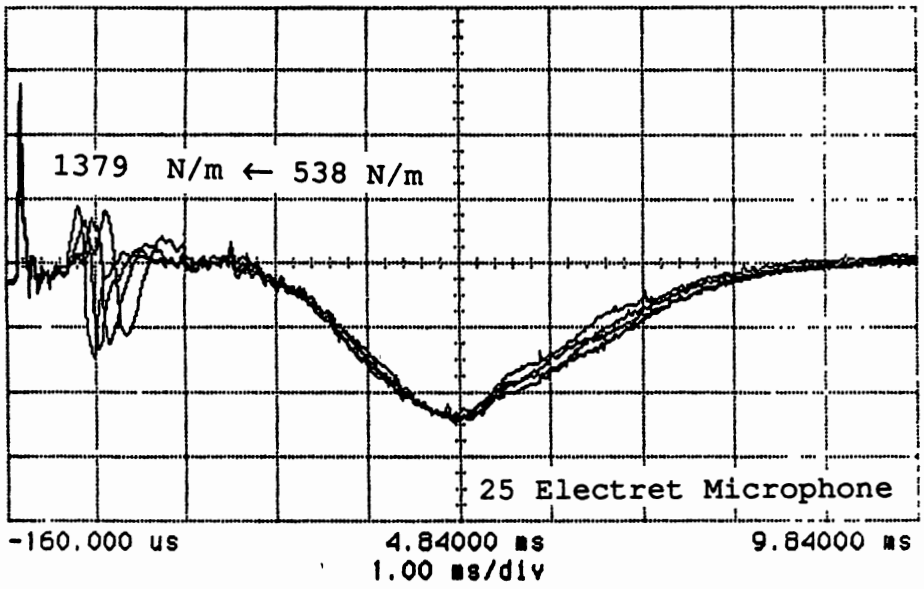

Figure 26. Pulse Waves in Mylar Tape with Tensions from 538 to 1379 N/m^2 with 280 N/m^2 Increments

4.6 Dispersion of Single Pulse Wave

To understand more about why waves propagate the way they do, it is necessary to find out more about the dispersion effect on a single pulse. Even though the waves formed in the web and excited by air pulse are not really rectangular shapes, for simplicity in analysis they are assumed so. The duration of a single pulse is selected to be 0.25 msec, as shown in Figure 27 (a). By Fourier transformation, a single pulse wave is composed by infinite odd number of frequency components. These frequency components are 1ω, 3ω, 5ω, 7ω, etc., and their corresponding relative amplitudes are 1, 1/3, 1/5, 1/7, etc., as shown in Figure 27 (b) to (e). As mentioned in chapter II, different frequencies travel at different velocities. Therefore, it is required to find out the corresponding velocity for each frequency component, which is calculated and shown in Appendix I. The calculation is based on the tensioned-plate model for the 3M recording medium at 525 N/m (3 pli) tension. With a 0.25-msec duration single-pulse wave, the fundamental frequency is 2 KHz. The corresponding velocity is 64.5 m/sec, and the other odd multiple harmonic frequency components (up to 4th harmonic, i.e. 14 KHz) are listed in Figure 27. Assume that the traveling distance of the pulse wave is 0.3 meters. Adding up the amplitudes for the frequency components (terminated waves) according to their corresponding speed of sound generates the final wave form shown in Figure 28. This final wave form provides an

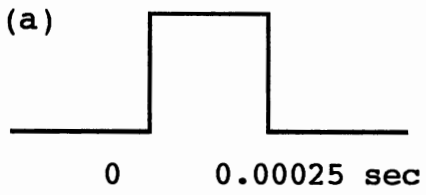

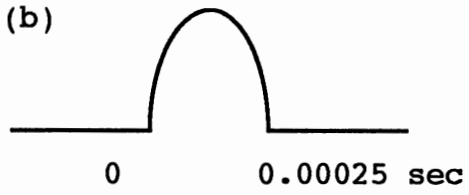

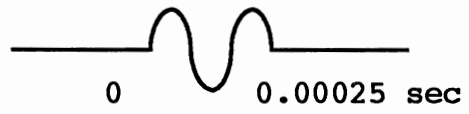

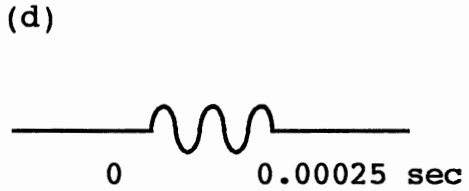

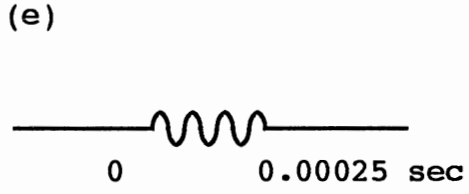

Frequency	Phase Velocity, Vph Tensioned Plate Model with Air-loading
Multi	
2000 Hz	64.5 m/sec
6000 Hz	69.0 m/sec
10000 Hz	70.8 m/sec
14000 Hz	70.8 m/sec

Figure 27. Pseudo Frequency Components of Single Pulse Wave and Their Corresponding Velocities

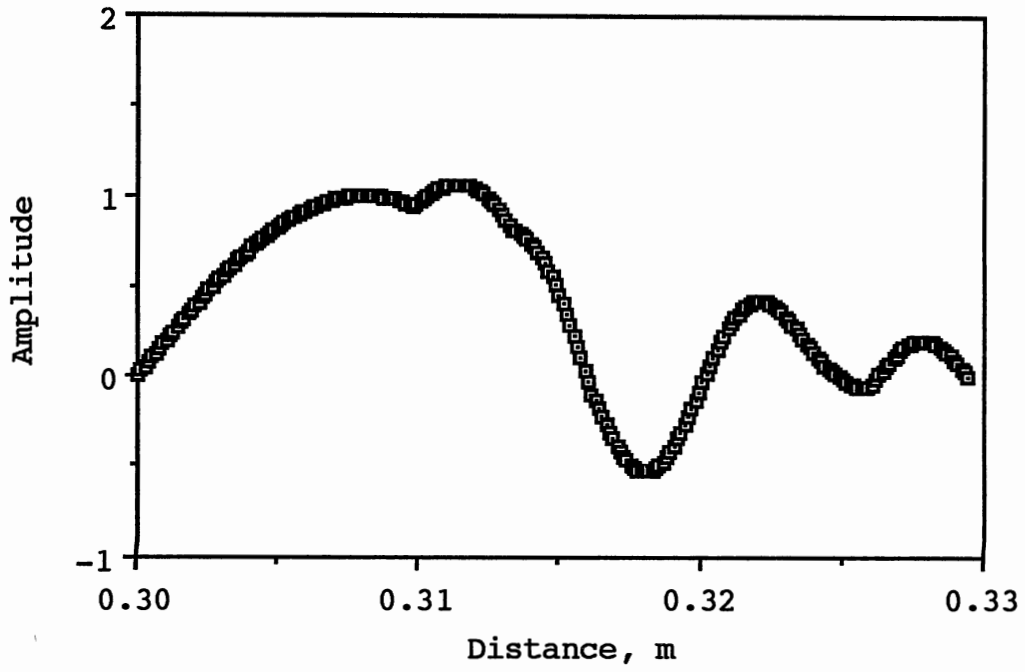

Figure 28. Dispersion Effect of Single Pulse Wave

explanation for the forerunners and also clearly indicates that the 3M recording medium is very dispersive. Experimental results also show the presence of forerunners. This is because the higher frequency component travels faster than the lower frequency one. But as we examine the experimental wave forms, the amplitude and the shape of the main signal are reduced and widened as the wave travels farther. This can not be simply explained by using the pseudo terminated waves model. In order to have a more complete explanation for forerunners, we need to use in the analysis all of the real frequency components associated with continuous waves.

4.7 Comparison of Pneumatic and Mechanical Excitations

By modifying the point-source system by adding a barrel in front of the pulser tube, a BB bullet can be shot to a web at much lower pressure without breaking but exciting the web mechanically. Figure 29 shows the laser vibrometer output signals with pneumatic and mechanical excitation methods. In this figure (a) and (b) are the signals recorded directly above the point of excitation of the 3M recording medium. The tension is set at 193 N/m (1.1 pli) in both cases. The wave excited by pulser tube is seen to have the shorter duration (about 0.4 msec). The shape of the wave is more like a one-complete cycle triangular wave. On the other hand, the wave excited by the BB bullet lasts 3.6 msec. The positive amplitude is much higher than the negative one. However, the wave generated by a BB bullet has a much sharper front edge.

Figure 30 shows the signals 4 inches downstream from the excitation point. Both waves indicate that higher frequency components arrive much sooner than the low frequency ones. The amplitudes keep increasing until merging into the main signals. Even these two input waves are not quite the same, but in both cases forerunners have been obtained. Forerunners do exit no matter by which method a web is excited. To show that the air blast from the mechanical excitation is not required for producing forerunners, one can simply throw a BB ball by hand. The same kind of results are

(a)

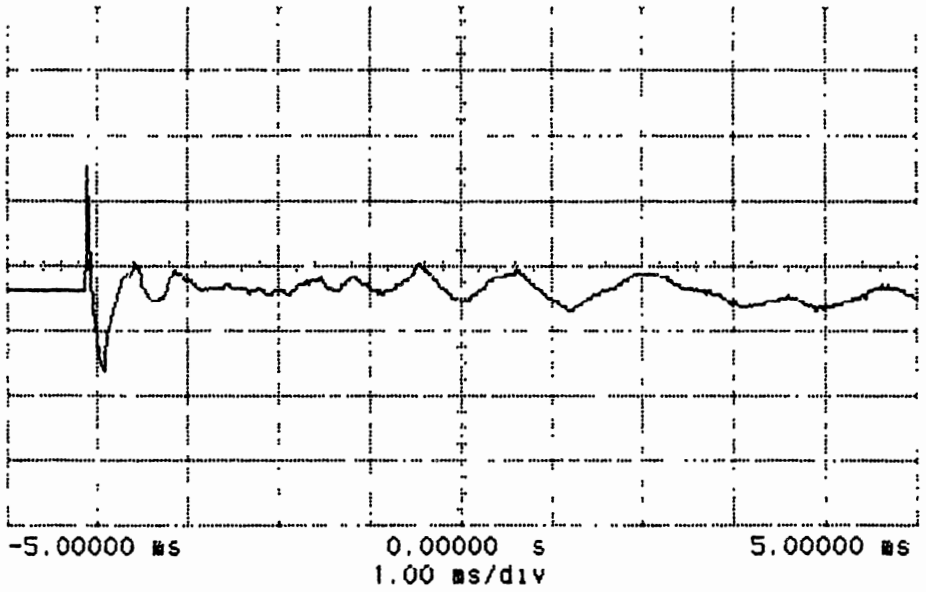

(b)

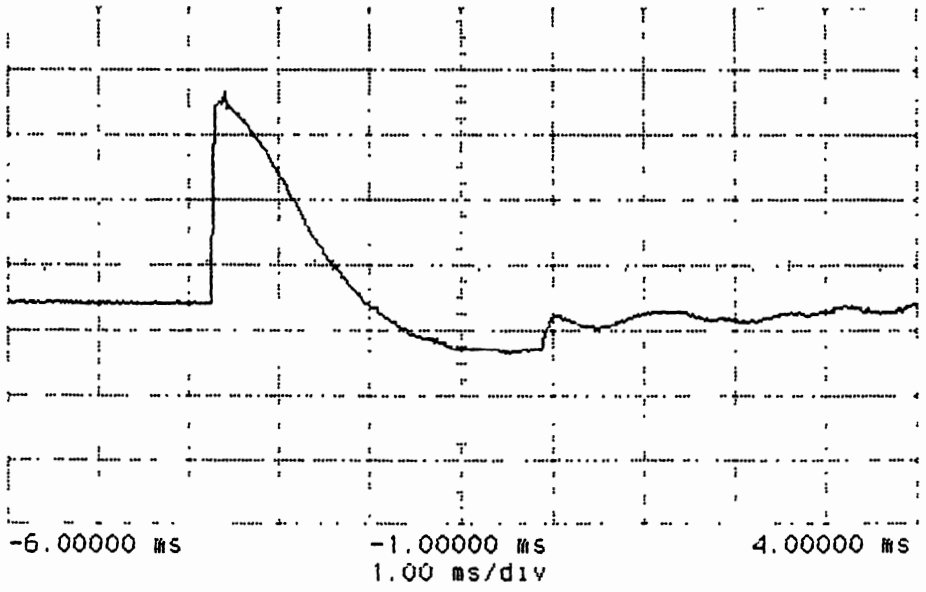

Figure 29. Laser Vibrometer Output Signals recorded directly above the excitation point with
(a) Pneumatic (Point-Source System)
(b) Mechanical Excitation Method

(a)

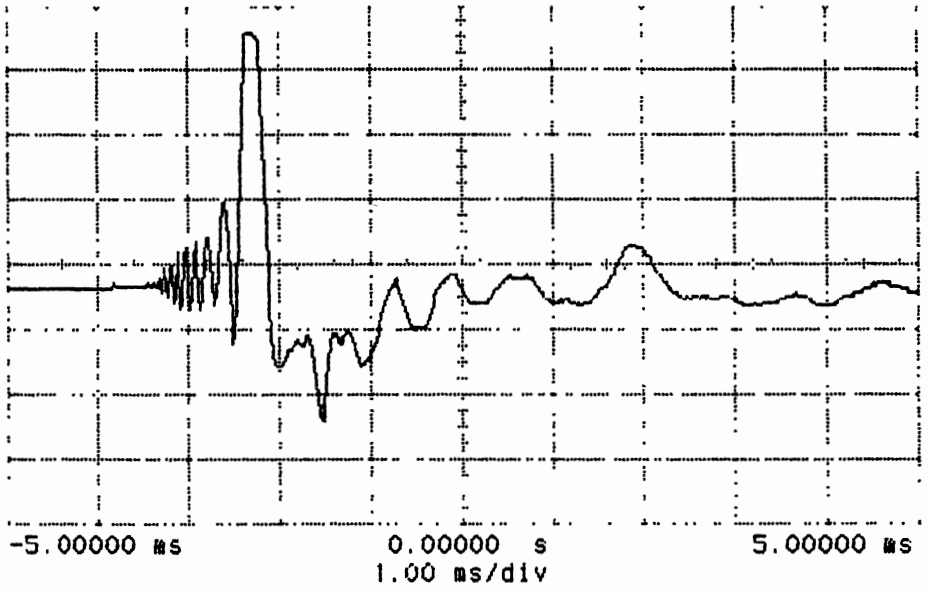

(b)

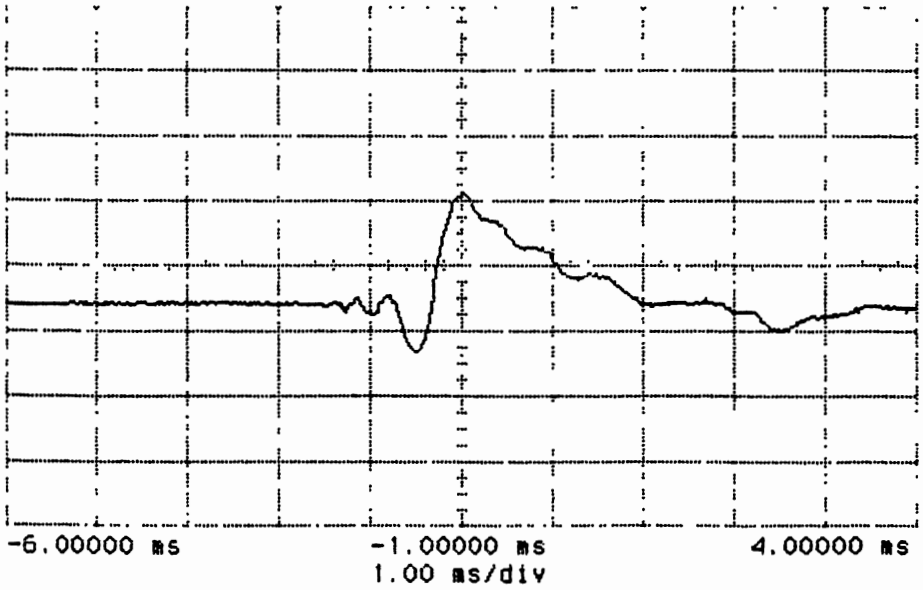

Figure 30. Laser Vibrometer Output Signals recorded 4 inches downstream from the excitation point with
(a) Pneumatic (Point-Source System)
(b) Mechanical Excitation Method

obtained as those produced by the mechanical excitation method. However, hand throwing of a BB ball is difficult to control.

The waves propagate two-dimensionally but mainly in the machine direction where the tension is applied. In both cases of mechanical and point-source excitation, the waves traveling in cross direction are much weaker than the ones having traveling the same distance in the machine direction. When the waves are much farther away in the machine direction (e.g. 11 inches from the excitation point), the amplitudes are not much different from those arriving in different cross-direction locations.

As shown in Figure 31, when the pulser-tube orientation is located in the machine or the cross direction, air blast from the pneumatic pulser does not make much difference in the velocity signals detected just above the excitation point. However, when the waves travel downstream in machine direction (Figure 32), the one excited in machine direction shows a much stronger and clearer forerunner signal.

4.8 Comparison of Experimental Results with Mathematical Function for Forerunners

As can be seen from oscilloscope traces detected by OPTEK (displacement sensor) and laser vibrometer (velocity sensor), forerunners or precursors gradually increase in amplitude and decrease in frequency with time. As shown in

(a)

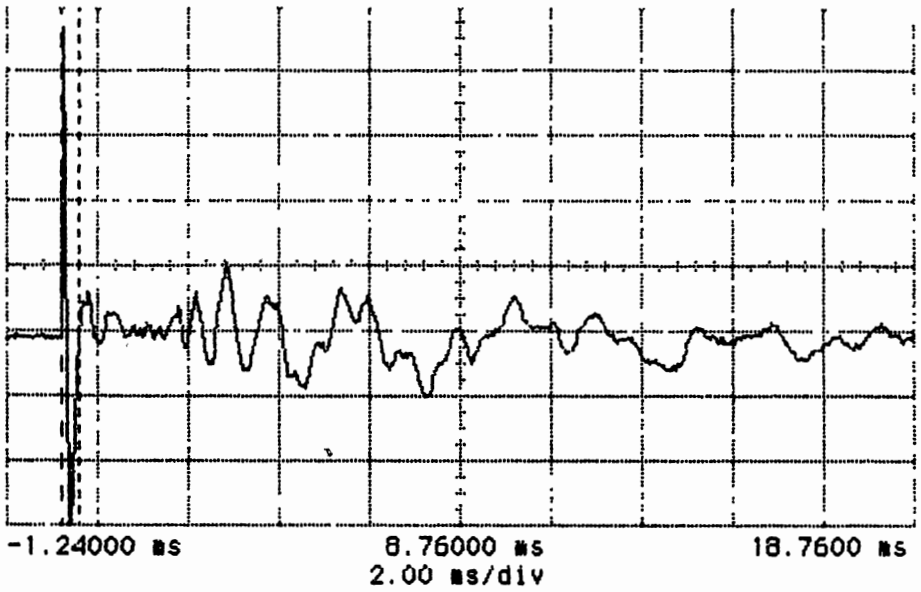

(b)

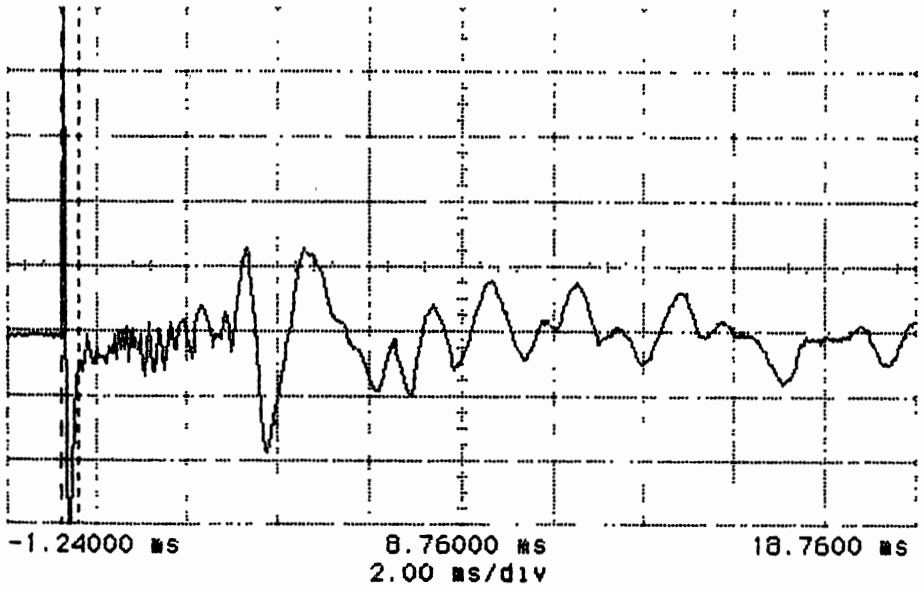

Figure 31. Laser Vibrometer Output Signals recorded directly above the excitation point where pulser tube in
(a) machine direction
(b) Cross direction

(a)

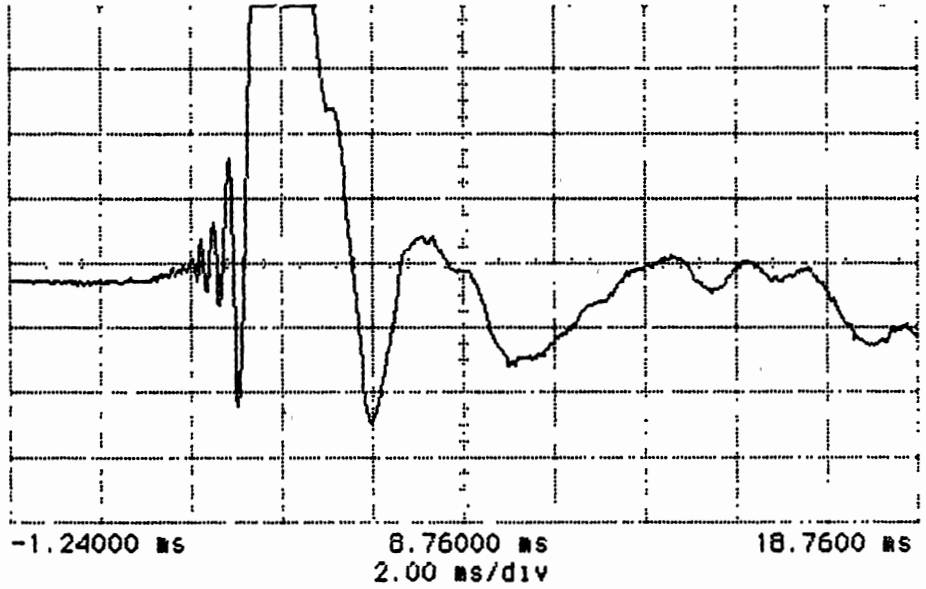

(b)

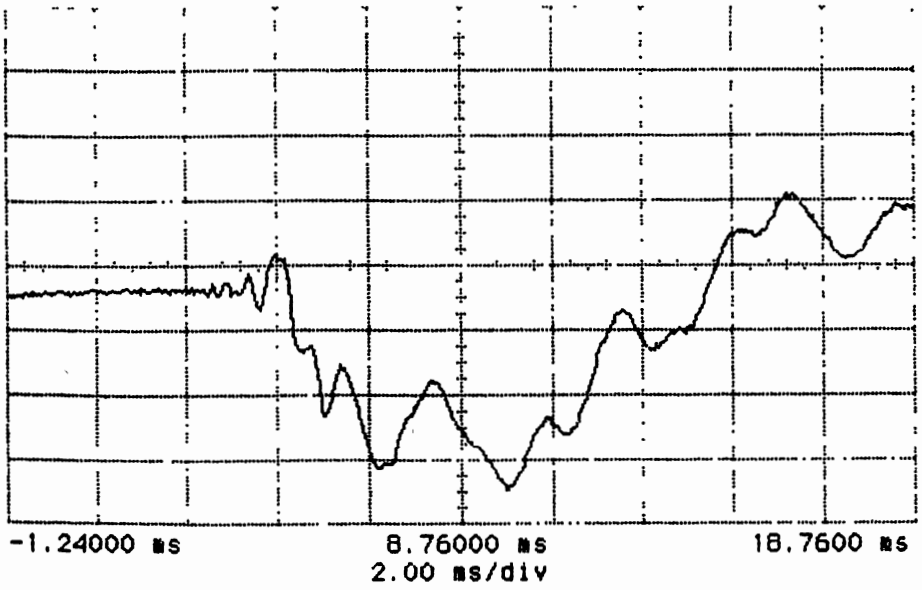

Figure 32. OPTEK's Output Signals recorded downstream from the excitation point where pulser tube in (a) machine direction (b) Cross direction

Figure 20, forerunners (precursors) seems to start at the same location no matter what tension is applied. This could be caused by the lack of high sensitivity or frequency-response in the equipment or forerunners, as it appears, might in deed start at the same location. Brillouin (13) states that the very beginning of the forerunners (precursors) is the front velocity. In optics, the front velocity should proceed as light velocity. Therefore, the front velocity of these precursors might proceed as the velocity of sound. In other words, the forerunners (precursors) might have the same beginning. This might be demonstrated if there were a equipment that could observe the infinitesimally small wave in intensity and wavelength.

Since it has been shown by Brillouin that classical forerunners can be described mathematically by a Bessel function of the first order, an attempt was made to reproduce the forerunners plot from the Bessel function. By using numerical recipes and assuming an incident period 0.5 msec, the shape of the displacement function shown in Figure 33 was obtained. Obviously, the calculated plot does not agree with that of experimental trace from the OPTEK sensor. The Bessel function of the first order increase its amplitude too fast. Since the agreement of the displacement function is not quite satisfactory, a second check was made to see if the first derivative of the Bessel function match the shape of the oscilloscope trace from the laser vibrometer. Therefore, the derivative of the displacement function was taken with

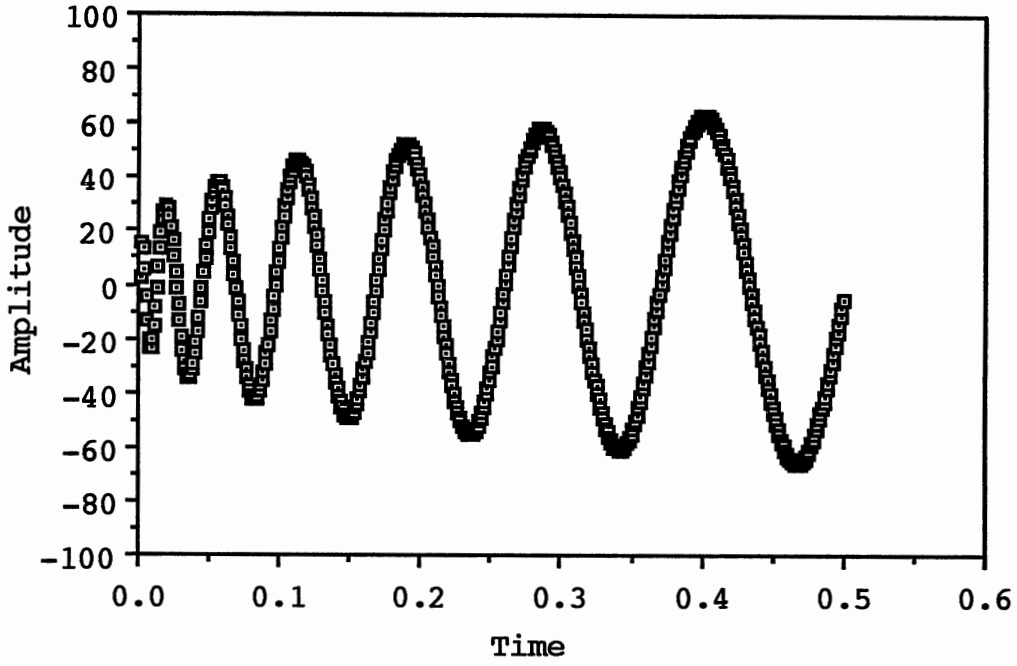

Figure 33. Displacement Function (Bessel Function of First Order)

respect to time to obtain the velocity which is the Bessel function of zero order. The velocity function so obtained was plotted out as shown in Figure 34. Its amplitude and frequency can be seen to decrease at the same time. Such a decreasing amplitude is opposite to the output trace from the laser vibrometer. Therefore, the results are not encouraging.

In order to see the relationship between tension and forerunners (precursors), the increasing amplitudes and periods were measured point by point. Figure 35 shows the average number of periods of forerunners from each individual oscilloscope trace of laser vibrometer for various tensions.

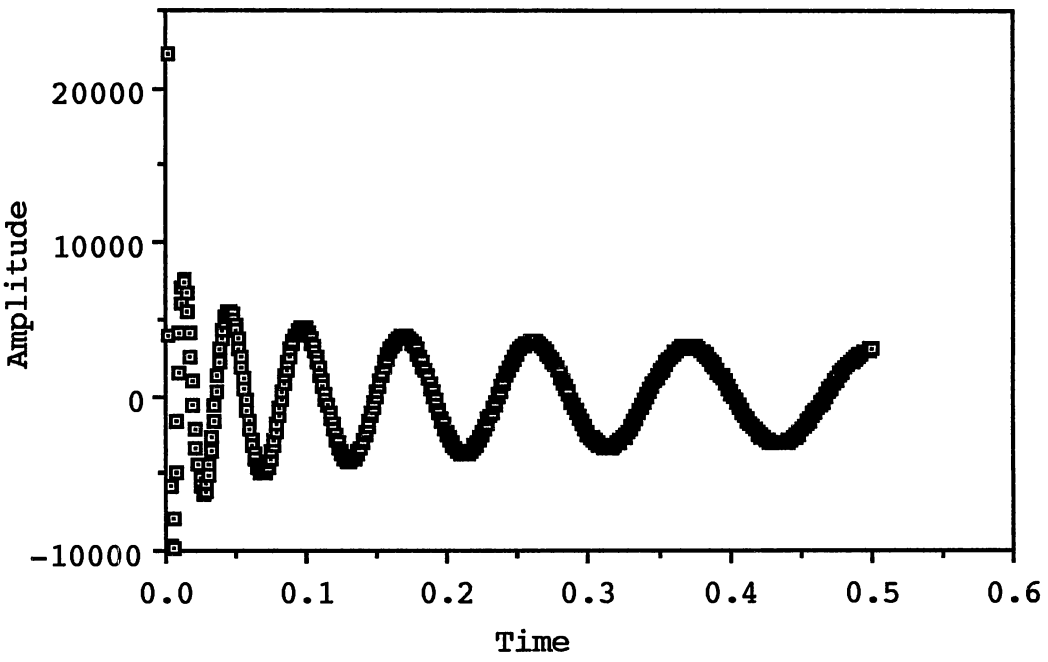

Figure 34. Velocity Function (Bessel Function of Zero Order)

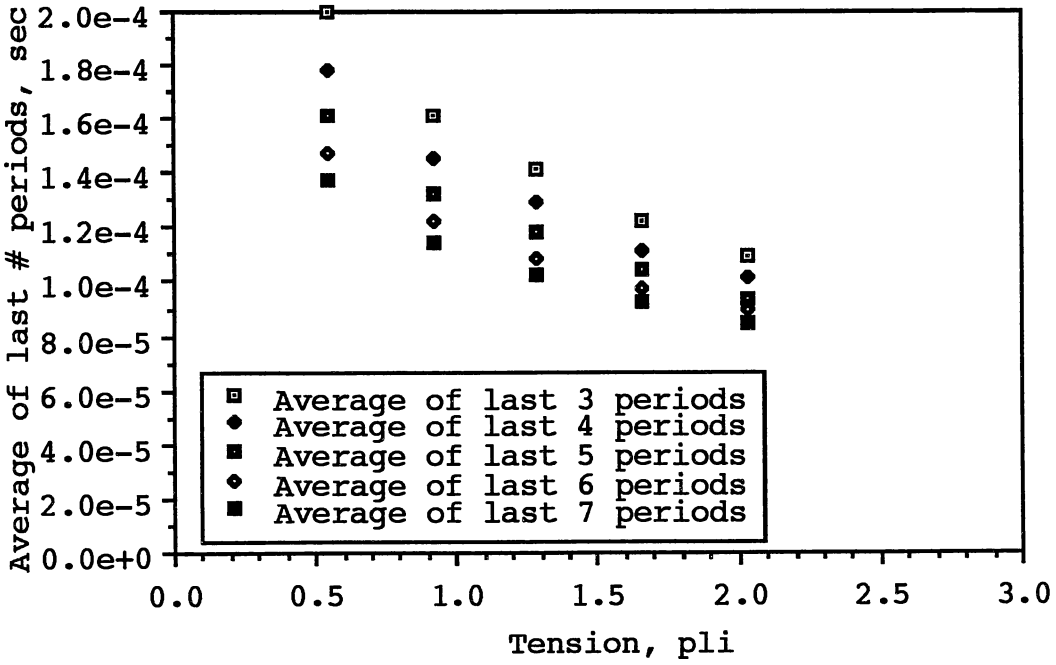

Figure 35. Relationship of Tension and Average Periods of Forerunners

CHAPTER V

SUMMARY AND FINDINGS

This investigation was initiated to develop a method for measuring the tension in an acoustically vibrated web. It was found from early experiments that the main wave form was preceded by a "forerunner" wave train which gradually increased in amplitude and decreased in frequency as it passes any given point. The first part of the research was to see if the point-source process could be used with a variety of web materials. The research also studied the factors affecting the operation of the point-source process, such as orientation of the pulser tube, pressure of air source, the spacing of the web and the pulser tube, and the tension of the web. Literature and modified models of wave propagation in membrane and plate were examined and compared with experimental data. The second part of the research was a study of the forerunner phenomenon mathematically with the ultimate aim of establishing a relation for use in measuring tension.

Two methods were used to generate waves in the webs. These were the speaker system and the point-source system. The speaker system allows one to generate single-frequency terminated waves since then there will be no problem in

defining phase velocity. Therefore, all the models can be checked with this system. Four models were examined, which included string, tensioned-beam model, membrane model with air-loading, and tensioned-plate model with air-loading. It was concluded that the tensioned-beam model predicted tension close to the actual tension (measured by dead weight). For a fixed value of tension, all the models but the tensioned-plate model with air-loading predicted increasing tensions as frequency increases. The reason that the tensioned-plate model with air-loading is different from the other is that it includes a consideration of tension, plate stiffness, and air mass. When the air mass is included, the tensioned-plate model and membrane model both predict tensions much higher than the actual tension. Especially, for the membrane model, the inclusion of air mass introduces the greatest error. In the tensioned-plate model, the plate stiffness term tends to compensate for the tension and air mass terms in predicting tension with increasing frequency. Inclusion of these three terms improves the tensioned-plate model with air-loading to predict tension consistently and independent of the input operating frequencies. A constant correction factor might be added to improve the agreement.

When placing a plexiglass plate directly above a web, it was found that the traveling velocity of the wave in the web decreased as the distance between the plate and the web increased. This shows that air mass can play a significant role.

The point-source process for wave generation induces a complex short-duration pulse wave into a web. This high-frequency pulse wave is composed of an infinite number of frequencies. Therefore, when defining the time of flight of the traveling wave, one should be aware that it is the group velocity that is obtained but the phase velocity should be used in the analysis of any models. However, to find phase velocity from the group velocity, the mean frequency of the pulse wave must be known and might be critical.

As discussed in the chapter IV, many factors influence the point-source process. The orientation of the pulser tube can change the amplitude and duration of the input pulse wave. The cross and machine directions, however, avoid the influence of air dynamic effect so that tension then became the principal variable. The normal direction is therefore not recommended for use because of its complexity. Furthermore, in testing soft web materials like tissue paper, the cross and machine directions are certainly recommended. With these directions there is no problem like that occasionally found for the normal direction in deforming or breaking the web by impinging the air directly into the web. Thus, there is no need to reduce the pressure of air source. As mentioned earlier, there are other factors that can affect the point-source process, such as the pressure of air source and the distance between the pulser tube and the web. All the materials have been tested with the point-source process successfully.

Since in the point-source process forerunners were observed in stiffer webs, an attempt was made to represent the wave form of forerunners by the first-order Bessel function. The results are not encouraging. The shape of displacement waves plotted by this mathematical function do not agree very well with experimental oscilloscope traces. Besides, the velocity trace obtained from the laser vibrometer is totally different from the plot obtained by differentiating the displacement with time. But the experimental results leave no doubt but that forerunners exist regardless of which excitation method (mechanical or point-source process) the web is excited by as long as the input wave is not purely single frequency and travels in a dispersive web. The wave propagates in two dimensions but mainly in the machine direction where tension is applied.

The wave front of the forerunners (precursors) starts much earlier than the main signal. From the experimental results, it appears that the front velocity of the precursors is independent of the web's tension. The measurable front velocity is 70% faster than the main signal velocity. Actually, the wave front is of very small amplitude and composed of high frequency wave. The highest frequency detected is 17 KHz. The small amplitude of the beginning wave is close to the noise level, and therefore, it is hard to detect.

5.1 Conclusions

Based on the experimental results and mathematical work, it can be concluded that:

1. In a pulse-excited web, the resultant wave is seen to be composed of two distinct parts: a high frequency "forerunner" wave in which the frequency progressively decreases and the amplitude increases, and a lower frequency main wave.

2. Forerunner waves can exist in web materials having thickness on the order of 0.003 inch or more and moduli of elasticity on the order of $5*10^5$ psi or more.

3. The formation of forerunner waves is related more to the rise time of the exciting pulse than it is to the duration of the pulse.

4. For the main part of the wave, the tensioned-plate model with air-loading adequately describes the relationship between tension and wave propagation velocity (phase velocity).

5. The response of the forerunner wave is less well understood, but the following may be concluded: (a) For a given distance from the pulser, the apparent average frequency of the four or five largest distinct cycles of the forerunner wave is strongly related to tension. As the tension is increased, the apparent period of each of the sinusoidal waves composing the forerunner decreases thus indicating an increase in instantaneous frequency. This relationship could provide the basis for a new type of

single-point tension measuring system. (b) For a given tension the wave propagating down the web in the machine direction shows an increase in overall length of the pulse envelope. The wavelets making up the forerunner show a decrease in frequency with distance.

6. The leading edge of the forerunner waves is difficult to detect because of the short wave lengths but frequencies of up to 17 KHz have been detected by the laser vibrometer. The point of origin of the forerunner waves is difficult to locate since the small amplitude waves dip below noise level, but it appears that the beginning of each measurable portion of the forerunner is seen to propagate at a velocity about 77% higher than the group velocity of the main part of the wave. As stated in chapter II, the group velocity for a pure plate with no tension is theoretically twice the phase velocity. However, for the tensioned-plate model or with air-loading, this statement is not valid and the group and velocities have much more complex relationship because of tension and air-loading effect.

7. The velocity of propagation of the main body of the wave is related to the amplitude of excitation although this effect cannot be quantified at this time. The type of nonlinearity formed in wave's response to various air pressure source cannot be explained solely by the tensioned-plate model with air-loading. This is probably due to two considerations: (a) The amplitude of excitation is much higher than can be analyzed by conventional linear plate

theory. Also for the tensioned-plate model with air-loading, the assumption is made of that no longitudinal particle motion is present; (b) The model is also based on the assumption of a plane wave front, which cannot exist in this case since the web is excited at a point instead of across the entire "ribbon". At the large amplitudes measured in these tests one must conclude that some coupling may exist between lateral and longitudinal motions. Such models exist for the large amplitude motion of strings but not for the large amplitude motion of a tensioned plate.

8. Forerunner waves are not related to any type of acoustical coupling between the sound wave produced by the pneumatic pulse. The waves can be excited easily by purely mechanical excitation.

9. Even though the waves propagate in two dimensions, most of the energy of the forerunners as well as that of the main waves propagates in a narrow channel in the machine direction.

10. Forerunner waves can be excited more strongly when the pulser tube is oriented in the machine direction than in the cross direction.

11. The formation of a strong tone-burst pulse having a frequency range beyond 5 KHz is almost impossible to achieve by non-contact means. Existing electro-mechanical exciters generally have piston areas too large to excite the small wavelengths required. Therefore, the pneumatic pulser developed through this work remains the best means of

exciting the web for non-contact tension measurement.

12. The tensioned-plate model with air-loading shows that the phase velocity of the web is related to the frequency of excitation, for a given tension, in three distinct regions (Figure 40). Region I, at low frequencies, is similar to the membrane model with air-loading. Region II, at intermediate frequencies, is controlled by plate, air, and membrane effects. While region III, which is at very high frequency, seems to be controlled by the stiffness of the web. Experimental verification of the tensioned-plate model with air-loading has been made for regions I and II (Figure 12) but the existing experimental system is incapable of detecting the high frequency waves needed to verify the application of the model to region III. Region III shows that the velocity of propagation increases with frequency. The frequencies at which region III begins in common webs might be as high as 10 to 20 KHz for low tensions. This effect might explain the formation of the front of the forerunner wave train which also has a very high propagation velocity. The instrumentation described here does not have the resolution to verify this effect.

13. Based on the investigation of the tensioned-plate model with the air-loading effect and with various type of materials, it can be concluded that the stiffness term is important, with the air-loading term probably less important in the absence of a nearby boundary. Other effects such as nonlinearity might exist.

5.2 Recommendations for Future Study

1. The phenomenon of coupled longitudinal and lateral motion in the tensioned-plate model with air-loading should be investigated both analytically and experimentally. A new experimental setup for doing this might include the use of a narrow metal "ribbon" onto which small strain gages could be mounted to measure high frequency longitudinal strains.

2. The formation of the head of the forerunner wave should be investigated experimentally. One possible method of doing this is to use Moiré fringe techniques or other optical methods.

3. The pulse excitation of the web results in waves propagating in the machine direction as well as in the cross direction. The shape of these waves is unknown, and while this information might be unimportant for tension measurement, the basic information would be valuable in understanding wave propagation in webs. The resultant wave patterns could probably be detected by Moiré fringe techniques, also.

4. One problem with the existing experimental setup has been that of easily controlling tension distribution in the static web. A new test machine should have a simple means of adjusting the tension distribution mechanically; i.e. finding a better means of controlling the reference tension.

5. The relationship between the mean frequency of the main body of the forerunner wave and the tension should be explored. A digital sampling system might be used to window

the main part of the forerunner so that the average period or frequency of the waves could be measured and related to tension.

6. The new tensioned-plate model with air-loading, should now be incorporated with the data acquisition system of the on-line tension measuring machine (36). This would allow measurements to be made for a much wider range of web thickness than is now possible.

BIBLIOGRAPHY

1. Meinander, S. and Marttinen, T., "Measuring of Web Tension Using Contactless Tension Meter," Graphics Arts Finland, Vol. 11, No. 1, pp. 34, 1982.

2. Linna, H. and Moilanen, P., "Comparison of Methods for Measuring Web Tension," Tappi Journal, Vol. 71. No. 10, pp. 134-138, 1988.

3. Marttinen, T. and Luukkala, M., "An Acoustic, Noncontacting Instrument to Measure Tension in a Moving Paper Web," 1985 IEEE Ultrasonic Symposium, pp. 553-556.

4. Linna, H., Moilanen, P., and Koskimies, J., "Web Tension Measurements in the Paper Mill," Proceedings of the First International Conference on Web Handling, Stillwater, Oklahoma, May, 1991

5. Karlsson, H., and Strom Valter, "STFI's Web Tension Indicator," Swedish Forest Products Research Laboratory, 1986.

6. Hansen, A., "A Portable Instrument for Web-Tension Control and Cross-Profile Recording," Tappi Journal, Vol. 69, No. 12, pp. 48-51, 1986.

7. Rye T. W., "Using TENSCAN to Measure the Tension Profile," Tappi Proceedings - 1988 Finishing and Converting Conference, pp. 175-178.

8. Ilvonen, P. and Vierimaa, P., "Wrinkles: Present Problem or Past," Proceedings of World Pulp and Paper Week, Book: Control Maintenance Environment, EUCEPA, pp. 151-158, 1990.

9. Kilmister, G. T. F., and Malinen, U., "The Measurement of Cross Machine Tension Distribution in a Paper Web during Manufacture," Proceedings of World Pulp and Paper Week, Book: Control Maintenance Environment, EUCEPA, pp. 141-149, 1990.

10. British Patent 1.160.112.

11. Jenkins, F., Fundamentals of Optics, McGraw-Hill, pp. 474-495, 1976.

12. Stumpf, F. B., Analytical Acoustics, Ann Arbor Science Publishers, Inc., pp. 5-18, 1981.

13. Brillouin, L., Wave Propagation and Group Velocity, Academic Press, 1960.

14. Elmore, W. C., and Heald, M. A., Physics of Waves, McGraw-Hill, pp. 114-127, 1969.

15. Merhaut, J., Theory of Electroacoustics, translated by Gerber, R., McGraw-Hill Inc., pp. 57-60, 1981

16. Morse, P. M. and Ingard, K. U., Theoretical Acoustics, McGraw-Hill Book Co., pp. 175-222, 1968.

17. Merilainen, P., "Propagation and Excitation of Membrane Waves Loaded by Air," Microwaves Optics and Acoustics, Vol. 2, No. 5, pp. 147-152, 1978.

18. Luukkala, M., and Merilainen, P., "A Membrane Wave Delay Line," Electronics Letters, Vol. 14, No. 4, pp. 123-124, 1978.

19. Morse, P. M., Vibration and Sound, McGraw-Hill Book Co., pp. 151-216, 1948.

20. Lindsay, R. B., Mechanical Radiation, McGraw-Hill, pp. 172-195, 1960.

21. Rayleigh, J. W. S., The Theory of Sound, Vol. 1, Dover Publications, pp. 260-294, 1945.

22. Landu, L. D., and Lifshitz, E. M., Translated from the Russian by Sykes, J. B. and Reid, W. H., Theory of Elasticity, Pergamon Press, pp. 113-115, 1970.

23. Timoshenko, S., Vibration Problems in Engineering, Van Nostrand, pp. 374-375, 1955.

24. Hutchison, T. S., The Physics of Engineering Solids, Wiley, pp. 465-482, 1968.

25. Podlesak, M. and Lee, A. R., "Dispersion of Waves in Piano Strings," Journal of Acoustical Society of American 83(1), pp. 305-317, 1988

26. Hartwig, J., Badde, R., and Davis, K., "Development of Pneumatic Pulser", 1990

27. Operator's Manual for OFV-2600/OFV-350 Vibrometer System, Polytec.

28. Bradley, M. E., "Noncontact Tension Measurement in Webs by Acoustical Point-Source Excitation," Master's Thesis, Oklahoma State University, Stillwater, Oklahoma, 1988.

29. Chang, Y. B. and Moretti, P. M., "Interaction of Fluttering Webs with Surrounding Air," TAPPI proceedings, 1990 Engineering Conference, Book 1, Seattle, Washington, September 24-27, 1990.

30. Chang, Y. B., Fox, S. J., Lilley, D. G., and Moretti, P. M., "Aerodynamics of Moving Belts, Tapes, and Webs," Machinery Dynamics and Element Vibrations, The 1991 ASME Design Technical Conferences - 13th Biennial Conference on Mechanical Vibration and Noise, Miami, Florida, September 22-25, 1991.

31. Albareda, E., Toribio, E., Gorri, J. A., and Perez, R., "Simulation of Wave Propagation in Dispersive Media Using FFT," American Journal Physics, Vol. 58, No. 9, pp. 844-848, 1990.

32. Chu, S. and Wong, S., "Linear Pulse Propagation in an Absorbing Medium," Physical Review Letters, Vol. 48, No. 11, pp. 738-741, 1982.

33. Tanka, M., "Description of a Wave Packet Propagation in Anomalous Dispersion Media - a New Expression of Propagation Velocity," Plasma Physics and Controlled Fusion, Vol. 31, No. 7, pp. 1049-1067, 1989.

34. Tanka, M., Fujiwara, M., and Ikegami, H., "Propagation of a Gaussian Wave Packet in an Absorbing Medium," Physical Review A, Vol. 34, No. 6, pp. 4851-4858, 1986.

35. Leibovich, S.and Seebass, A. R., "Nonlinear Waves," Cornell University Press, pp. 212-234, 1974.

36. Vickery, C. M., "Use of Pneumatic Pulse Stimulus for Inducement of Large Amplitude Flexural Waveform in Web Materials for the Purpose of Local Tension Measurement," Ph.D. Dissertation, School of Mechanical and Aerospace Engineering, Oklahoma State University, Stillwater, Oklahoma, 1992.

APPENDIXES

APPENDIX A

MEMBRANE WITH AIR-LOADING MODEL*

The general equation of motion in one-dimension for a thin membrane under uniaxial tension is

$$T \frac{\partial^2 \eta}{\partial x^2} + F_\omega = \sigma_1 \frac{\partial^2 \eta}{\partial t^2} \tag{A.1}$$

Assume that solution for the displacement of the membrane has the following form:

$$\eta(x,t) = Ae^{j(Kx-\omega t)} \tag{A.2}$$

In the atmosphere, the reactive force of the surrounding air can be expressed as

$$F_\omega = (p_- - p_+)_{\eta=0} = -2Pe^{j(Kx-\omega t)} \tag{A.3}$$

where

$$\begin{cases} p_+ = Pe^{j(Kx-\omega t)}e^{-q\eta} & (\eta \geq 0) \\ p_- = -Pe^{j(Kx-\omega t)}e^{q\eta} & (\eta \leq 0) \end{cases} \tag{A.4}$$

The pressure wave has to satisfy the general wave equation in air:

$$\frac{\partial^2 p}{\partial x^2} + \frac{\partial^2 p}{\partial \eta^2} = \frac{1}{C^2} \frac{\partial^2 p}{\partial t^2} \tag{A.5}$$

The second derivatives of the pressure wave with respect to

---

*Rederivation from Merilainen, P., "Propagation and Excitation of Membrane Waves Loaded by Air", Microwaves Optics and Acoustics, Vol. 2, No. 5, pp. 147-152, 1978.

x, η, and t are

$$\begin{cases} \dfrac{\partial^2 p_+}{\partial x^2} = - PK^2 e^{j(Kx-\omega t)} e^{-q\eta} \\ \dfrac{\partial^2 p_+}{\partial \eta^2} = Pq^2 e^{j(Kx-\omega t)} e^{-q\eta} \\ \dfrac{\partial^2 p_+}{\partial t^2} = - Pw^2 e^{j(Kx-\omega t)} e^{-q\eta} \end{cases} \quad \text{or} \quad \begin{cases} \dfrac{\partial^2 p_-}{\partial x^2} = PK^2 e^{j(Kx-\omega t)} e^{-q\eta} \\ \dfrac{\partial^2 p_-}{\partial \eta^2} = - Pq^2 e^{j(Kx-\omega t)} e^{-q\eta} \\ \dfrac{\partial^2 p_-}{\partial t^2} = Pw^2 e^{j(Kx-\omega t)} e^{-q\eta} \end{cases} \tag{A.6}$$

Substitute Eqn. (A.6) into Eqn. (A.5) and obtain

$$(- K^2 + q^2) P e^{j(Kx-\omega t)} e^{-q\eta} = - \frac{\omega^2}{C^2} P e^{j(Kx-\omega t)} e^{-q\eta} \tag{A.7}$$

Solve for the attenuation constant (q) in air:

$$q = \sqrt{K^2 - k^2} \tag{A.8}$$

For continuity, the membrane velocity needs to equal the air particle velocity on the membrane surface. They are connected by the following equation:

$$- \rho \frac{\partial u}{\partial t} = \nabla p \tag{A.9}$$

i.e.

$$- \rho \frac{\partial (u_x i + u_\eta j)}{\partial t} = \frac{\partial p}{\partial x} i + \frac{\partial p}{\partial \eta} j \tag{A.10}$$

i.e.

$$\begin{cases} - \rho \dfrac{\partial u_x}{\partial t} = \dfrac{\partial p}{\partial x} \Rightarrow \quad u_x = \dfrac{K}{\rho \omega} p \\ - \rho \dfrac{\partial u_\eta}{\partial t} = \dfrac{\partial p}{\partial \eta} \Rightarrow \quad u_\eta = \dfrac{iq}{\rho \omega} p \end{cases} \tag{A.11}$$

In order to satisfy continuity condition, the traverse velocity of air particles is equal to that of the membrane at $\eta = 0$.

$$u_\eta|_{\eta=0} = \frac{\partial \eta}{\partial t} \tag{A.12}$$

Substitute Eqns. (A.11) and (A.2) into Eqn. (A.12), then

$$\frac{iq}{\rho\omega} p\Big|_{\eta=0} = \frac{\partial (Ae^{j(Kx-\omega t)})}{\partial t} \tag{A.13}$$

Replace the pressure wave with its amplitude and variation as shown in Eqn. (A.4)

$$\frac{iq}{\rho\omega} Pe^{j(Kx-\omega t)}e^{-q\eta}\Big|_{\eta=0} = - i\omega Ae^{j(Kx-\omega t)} \tag{A.14}$$

Solve for the amplitude of air pressure.

$$P = - \frac{\rho\omega^2 A}{q} \tag{A.15}$$

Substitute Eqns. (A.15) and (A.4) into Eqn. (A.1)

$$T \frac{\partial^2 \eta}{\partial x^2} + (- 2)(- \frac{\rho\omega^2 A}{q})e^{j(Kx-\omega t)} = \sigma_1 \frac{\partial^2 \eta}{\partial t^2} \tag{A.16}$$

Take second derivatives of the displacement function with respect to x and t, and rewrite Eqn. (A.16) as

$$T(iK)^2 Ae^{j(Kx-\omega t)} + \frac{2\rho\omega^2 A}{q} e^{j(Kx-\omega t)} = \sigma_1(-i\omega)^2 Ae^{j(Kx-\omega t)} \tag{A.17}$$

Cancel the common term, $Ae^{j(Kx-\omega t)}$ and obtain

$$- TK^2 + \frac{2\rho\omega^2}{q} = - \sigma_1\omega^2 \tag{A.18}$$

Then, solve for angular frequency, ω

$$\omega^2 = \frac{TK^2}{\sigma_1 + \frac{2\rho}{q}} \tag{A.19}$$

Substitute Eqn. (A.8) and $V_{ph} = \omega/K$ into Eqn. (A.19)

$$V_{ph}^2 = \frac{T}{\sigma_1 + \frac{2\rho}{\sqrt{K^2 - k^2}}} \tag{A.20}$$

Rearrange the above equation and then get the relationship between tension and velocity:

$$T = (\sigma_1 + \frac{2\rho}{\sqrt{K^2 - k^2}}) V_{ph}^2 \qquad (A.21)$$

APPENDIX B

TENSIONED-BEAM MODEL

The equation of motion for a tensioned beam is

$$T\frac{\partial^2\eta}{\partial x^2} - EI\frac{\partial^4\eta}{\partial x^4} = \sigma_1\frac{\partial^2\eta}{\partial t^2} \tag{B.1}$$

Assume that solution for the displacement of the tensioned beam has the following form:

$$\eta(x,t) = Ae^{j(\omega t-Kx)} \tag{B.2}$$

and its second and fourth derivatives with respect to x and t are

$$\begin{cases} \dfrac{\partial^2\eta}{\partial x^2} = -AK^2e^{j(\omega t-Kx)} \\ \dfrac{\partial^4\eta}{\partial x^4} = AK^4e^{j(\omega t-Kx)} \\ \dfrac{\partial^2\eta}{\partial t^2} = -A\omega^2e^{j(\omega t-Kx)} \end{cases} \tag{B.3}$$

Substitute Eqns. (B.3) back into Eqn. (B.1)

$$(-TK^2 - EIK^4)Ae^{j(\omega t-Kx)} = -\sigma_1\omega^2Ae^{j(\omega t-Kx)} \tag{B.4}$$

$$TK^2 + EIK^4 = \sigma_1\omega^2 \tag{B.5}$$

$$T\left(\frac{\omega}{V_p}\right)^2 + EI\left(\frac{\omega}{V_p}\right)^4 = \sigma_1\omega^2 \tag{B.6}$$

$$TV_p^2 + EI\omega^2 = \sigma_1V_p^4 \tag{B.7}$$

$$\sigma_1(V_p^2)^2 - T(V_p^2) - EI\omega^2 = 0 \tag{B.8}$$

Solve for phase velocity of plate, V_p

$$V_p = \sqrt{\frac{T + \sqrt{T^2 + 4\sigma_1 EI\omega^2}}{2\sigma_1}} \qquad \text{(B.9)}$$

and solve for tension, T

$$T = \sigma_1 V_p^2 - EI \frac{\omega^2}{V_p^2} \qquad \text{(B.10)}$$

APPENDIX C

SOLENOID VALVES TESTING

Several combinations of Eemco solenoid valves were tested to find the one that can provide the best acoustic signal. Table II lists the different parameters for the examined valves. An Electret microphone was located 2.25 inches apart from the pulser tube. The setup is similar to Figure 9 (b) except no web and only one microphone is used. The pulser tube is 86 inches long, and its inside diameter is 1/4 inch. The pulse generator is set at 3 ms and 106 ms for pulse width and spacing. The testing data show that the old Eemco valve produces the sharpest pulse in general.

TABLE II

EEMCO SOLENOID VALVES TESTING DATA

ORIFICE	SPRING	COIL	AIR PRESSURE	TIME μsec	AMPLITUDE mV
.09	.23		20	63	428
			30	60	769
			40	60	913
			50	58	935
			60	56	914
			64	57	927
.09	.023	4.8	20	60	516
			30	60	831
			40	58	919

			50	58	935
			60	56	919
			64	56	928
.06	.02	4.8	20	61	125
			30	60	316
			40	60	453
			50	59	563
			60	59	663
			64	59	694
.06	.02	regular	30	63	230
			40	60	397
			50	60	525
			60	59	644
			64	59	693
.06	.023	regular	30	61	278
			40	59	454
			50	57	574
			60	57	684
			64	57	705
.06	.023	4.8	30	57/59	356
			40	59	473
			50	59	592
			60	59	684
			64	59	711
old	old	4.8	20	57/58	85
			30	58	898
			40	58	906
			50	56	914
			60	58	602
			64	no pulse	
old	old	regular	20	59	750
			30	59	906
			40	57	906
			50	55	906
			60	no pulse	
old	.023	regular	20	59	694
			30	58	898
			40	56	898
			50	no pulse	
old	.023	4.8	20	56	820
			30	58	898
			40	56	898
			50	59	797
			60	no pulse	
old	.023	old	20	57	700
			30	56	914
			40	54	914
			50	56	664
old	old	old	20	60	641
			30	58	891
			40	56	914
			50	55	914
			60	no pulse	

APPENDIX D

SHAKER TESTS FOR MICROPHONE AND OPTEK SENSORS

A shaker has a vibrating surface with controllable frequency. By setting up a OPTEK and a Electret microphone to sense the motion, the result is shown in Figure 36. Since it was very noisy when operating the shaker, the microphone also picked up the noise. The result shows that peaks for each trace are in the same locations. The microphone's signal shows 180° out of phase with the OPTEK sensor's, instead of 90°. Therefore, the microphone is not a velocity transducer since the OPTEK sensor is a displacement transducer. Based on the amplitude change of the microphone's signals when frequency was increased, it seems that the microphone is a displacement transducer. Due to frequency and amplitude limitation of shaker, frequency was only able to be operated up to 300 Hz.

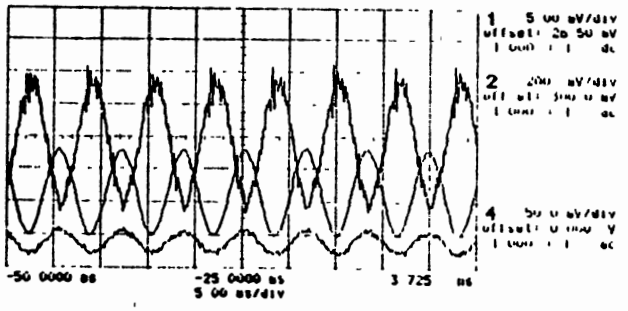

Figure 36. Signals of Electret Microphone, OPTEK Sensor, and Shaker

APPENDIX E

STATIC CALIBRATION CURVES FOR OPTEK MODEL OPB 125AL

To ensure the 3-mil paper is flat enough to do the calibration curves, tension is set at 2.65 pli. The distance between the web and the OPTEK sensor is adjustable by attaching the OPTEK sensor on a vertical traverse mechanism. Then, the static calibration curves are obtained by varying the distance and recording the output voltage, as shown

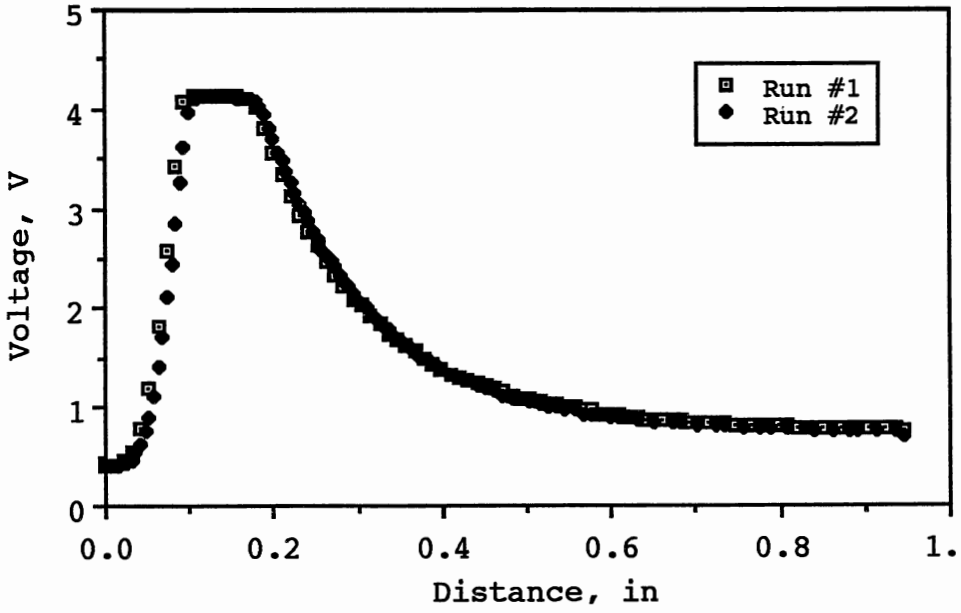

Figure 37. Calibration Curves for OPTEK Model OPB 125AL

APPENDIX F

SCHEMATIC AND BLOCK DIAGRAMS OF THE

POLYTEC LASER VIBROMETER SYSTEM

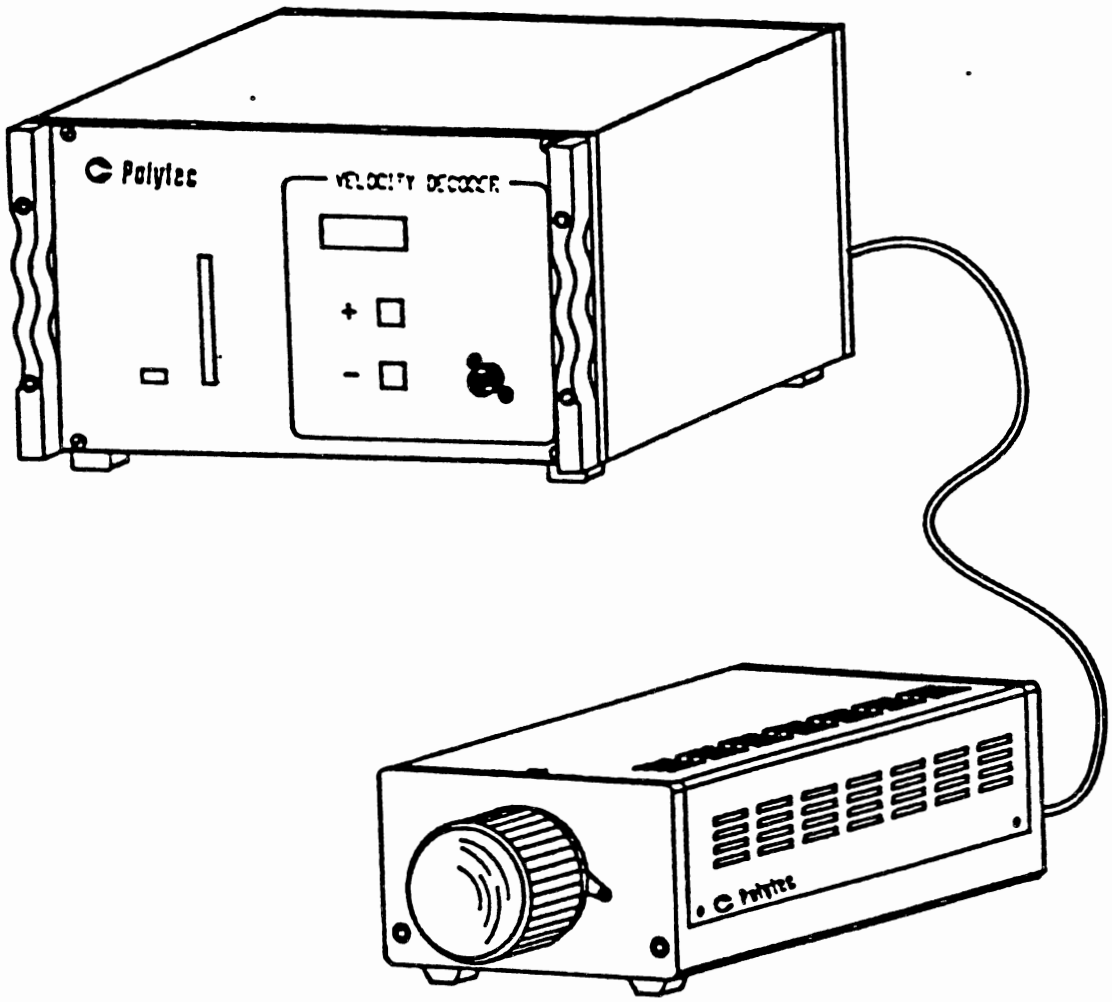

Source: Operator's Manual for OFV-2600/OFV vibrometer system, Polytec

Figure 38. Schematic Diagram of the Polytec Laser Vibrometer

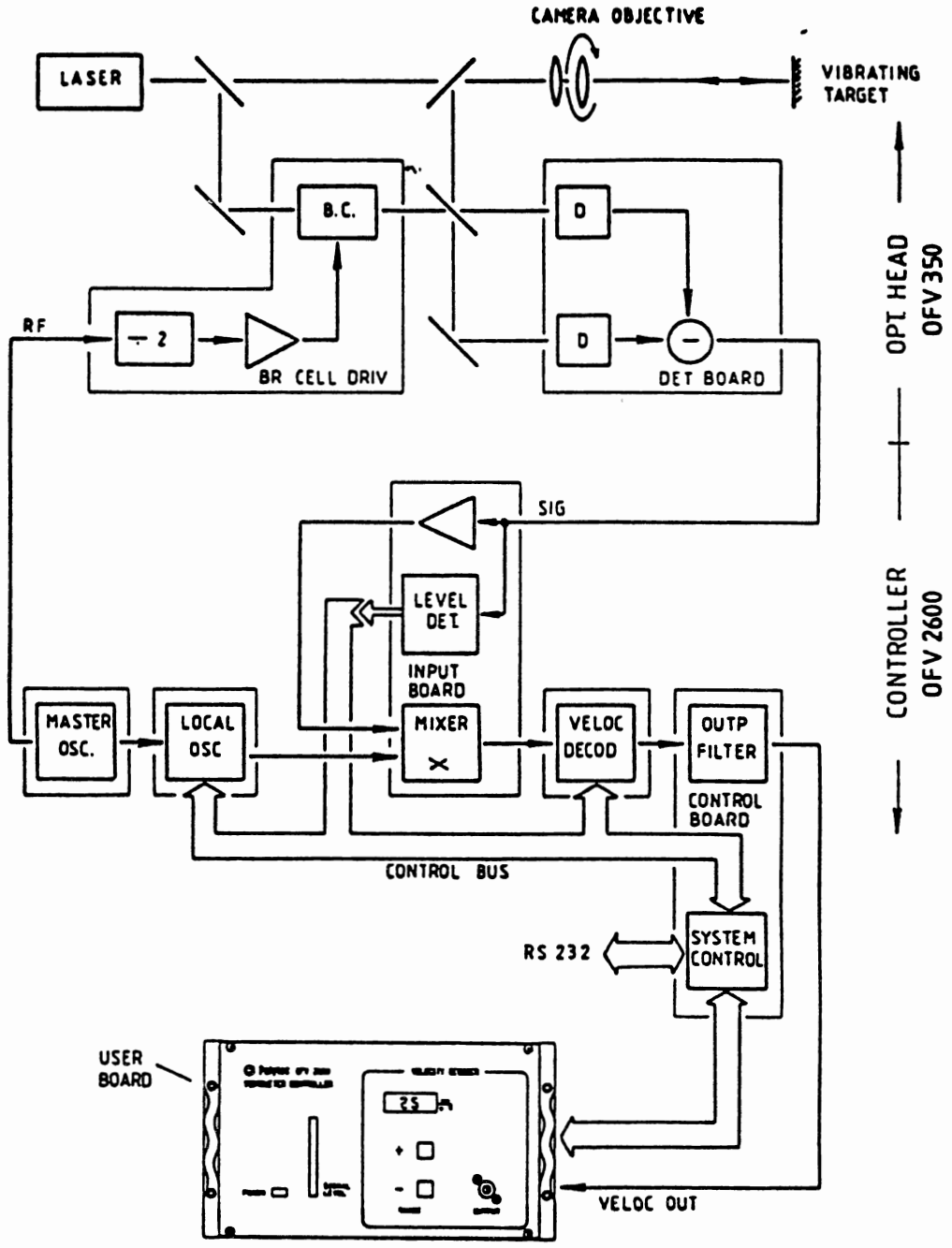

Source: Operator's Manual for OFV-2600/OFV vibrometer system, Polytec

Figure 39. Block Diagram of the Polytec Laser Vibrometer

APPENDIX G

TENSIONED-PLATE WITH AIR-LOADING MODEL

The general equation of motion in one-dimension for a tensioned plate is

$$T_1 \frac{\partial^2 \eta}{\partial x^2} - EI \frac{\partial^4 \eta}{\partial x^4} = (\sigma_1 + \frac{2\rho}{\sqrt{K^2 - k^2}} w) \frac{\partial^2 \eta}{\partial t^2} \tag{G.1}$$

Assume that solution for the displacement of the tensioned plate has the following form:

$$\eta(x,t) = Ae^{j(\omega t - Kx)} \tag{G.2}$$

and its second and fourth derivatives with respect to x and t are

$$\begin{cases} \frac{\partial^2 \eta}{\partial x^2} = - AK^2 e^{j(\omega t - Kx)} \\ \frac{\partial^4 \eta}{\partial x^4} = AK^4 e^{j(\omega t - Kx)} \\ \frac{\partial^2 \eta}{\partial t^2} = - A\omega^2 e^{j(\omega t - Kx)} \end{cases} \tag{F.3}$$

Substitute Eqns. (G.3) into Eqn. (G.1)

$$(T_1 K^2 + EIK^4) Ae^{j(\omega t - Kx)} = (\sigma_1 + \frac{2\rho}{\sqrt{K^2 - k^2}} w)\omega^2 Ae^{j(\omega t - Kx)} \tag{G.4}$$

$$T_1 K^2 + EIK^4 = (\sigma_1 + \frac{2\rho}{\sqrt{K^2 - k^2}} w)\omega^2 \tag{G.5}$$

$$T_1 (\frac{\omega}{V_{ph}})^2 + EI(\frac{\omega}{V_{ph}})^4 = (\sigma_1 + \frac{2\rho}{\sqrt{K^2 - k^2}} w)\omega^2 \tag{G.6}$$

$$T_1 V_{ph}^2 + EI\omega^2 = (\sigma_1 + \frac{2\rho}{\sqrt{K^2 - k^2}} w)(V_{ph}^4) \tag{G.7}$$

$$(\sigma_1 + \frac{2\rho}{\sqrt{K^2 - k^2}} w)(V_{ph}^2)^2 - T_1(V_{ph}^2) - EI\omega^2 = 0 \tag{G.8}$$

Solve for phase velocity, V_{ph}

$$V_{ph} = \sqrt{\frac{T_1 + \sqrt{T_1^2 + 4(\sigma_1 + \frac{2\rho}{\sqrt{K^2 - k^2}} w)EI\omega^2}}{2(\sigma_1 + \frac{2\rho}{\sqrt{K^2 - k^2}} w)}} \tag{G.9}$$

and solve for tension, T_1

$$T_1 = (\sigma_1 + \frac{2\rho}{\sqrt{K^2 - k^2}} w)V_{ph}^2 - EI \frac{\omega^2}{V_{ph}^2} \tag{G.10}$$

APPENDIX H

EXPERIMENTAL AND CALCULATED DATA FOR MEAD

80 LB SIGNATURE DULL

Table III

Experimental and Calculated Tensions for Mead 80 Lb. Signature Dull

TYPE OF WEB:	80# SIGNATURE DULL
WIDTH OF WEB:	0.1524 m
DENSITY OF WEB:	0.1213 Kg/m^2
THICKNESS OF WEB:	9.84E-05 m
YOUNG'S MODULUS:	7.32E+9 Pa
SPEED OF SOUND:	331.6 m/sec
DENSITY OF AIR:	1.21 Kg/m^3
DISTANCE OF SENSORS:	0.2032 m
MOMENT OF INERTIA:	1.21E-14 M^4

FREQ. Hz	TIME sec	VEL. m/sec	TENSION N/m				
			DEAD WEIGHT	STRING	MEM W/AIR	TENSION BEAM	BOTH W/AIR
298	7.56E-3	26.88	85.23	87.63	112.84	84.82	110.03
352	7.36E-3	27.61	85.23	92.46	115.56	88.73	111.83
403	7.32E-3	27.76	85.23	93.47	113.98	88.63	109.14
446	7.24E-3	28.07	85.23	95.55	114.69	89.74	108.89
500	7.16E-3	28.38	85.23	97.70	115.37	90.58	108.25
556	7.08E-3	28.70	85.23	99.92	116.37	91.32	107.77
595	7.04E-3	28.86	85.23	101.06	116.68	91.30	106.92
641	6.92E-3	29.36	85.23	104.59	119.86	93.66	108.93
694	6.84E-3	29.71	85.23	107.05	121.65	94.51	109.11
758	6.76E-3	30.06	85.23	109.60	123.47	95.03	108.89
806	6.68E-3	30.42	85.23	112.24	125.74	96.12	109.62
301	7.04E-3	28.86	114.42	101.06	131.92	98.56	129.42
352	6.76E-3	30.06	114.42	109.60	139.43	106.45	136.28
403	6.64E-3	30.60	114.42	113.60	141.09	109.61	137.11
446	6.60E-3	30.79	114.42	114.98	140.27	110.16	135.44
500	6.48E-3	31.36	114.42	119.28	143.14	113.44	137.30

543	6.44E-3	31.55	114.42	120.76	143.13	113.96	136.32
595	6.36E-3	31.95	114.42	123.82	145.02	115.86	137.06
658	6.28E-3	32.36	114.42	127.00	146.92	117.51	137.44
694	6.24E-3	32.56	114.42	128.63	147.87	118.19	137.44
758	6.16E-3	32.99	114.42	131.99	150.33	119.89	138.23
397	6.12E-3	33.20	143.60	133.72	169.43	130.45	166.15
455	6.08E-3	33.42	143.60	135.49	167.28	131.24	163.04
500	6.04E-3	33.64	143.60	137.29	166.77	132.22	161.70
543	5.92E-3	34.32	143.60	142.91	171.72	137.16	165.97
610	5.80E-3	35.03	143.60	148.89	176.20	141.94	169.25
658	5.72E-3	35.52	143.60	153.08	179.48	145.21	171.61
694	5.68E-3	35.77	143.60	155.24	180.79	146.60	172.14
758	5.64E-3	36.03	143.60	157.45	181.37	147.31	171.23
806	5.60E-3	36.29	143.60	159.71	182.67	148.38	171.33
847	5.58E-3	36.42	143.60	160.86	182.94	148.43	170.51
893	5.54E-3	36.68	143.60	163.19	184.61	149.59	171.01
943	5.50E-3	36.95	143.60	165.57	186.29	150.61	171.33
1000	5.46E-3	37.22	143.60	168.01	187.98	151.44	171.42
403	5.52E-3	36.81	172.79	164.37	212.32	161.62	209.56
455	5.48E-3	37.08	172.79	166.78	210.25	163.33	206.81
500	5.40E-3	37.63	172.79	171.76	213.07	167.71	209.02
543	5.36E-3	37.91	172.79	174.33	213.20	169.62	208.48
610	5.32E-3	38.20	172.79	176.96	212.40	171.12	206.55
658	5.28E-3	38.48	172.79	179.66	213.25	172.95	206.55
694	5.24E-3	38.78	172.79	182.41	214.97	175.05	207.62
758	5.20E-3	39.08	172.79	185.23	215.78	176.60	207.15
806	5.20E-3	39.08	172.79	185.23	213.92	175.45	204.15
862	5.18E-3	39.23	172.79	186.66	213.82	175.58	202.74
909	5.16E-3	39.38	172.79	188.11	214.17	175.88	201.94
943	5.14E-3	39.53	172.79	189.58	214.98	176.51	201.92
1000	5.14E-3	39.53	172.79	189.58	213.54	174.89	198.86
397	5.16E-3	39.38	201.98	188.11	247.80	185.78	245.47
446	5.20E-3	39.08	201.98	185.23	237.07	182.23	234.07
500	5.12E-3	39.69	201.98	191.06	239.56	187.42	235.92
543	5.08E-3	40.00	201.98	194.08	239.77	189.84	235.53
595	5.04E-3	40.32	201.98	197.17	239.90	192.17	234.89
658	5.00E-3	40.64	201.98	200.34	239.93	194.33	233.92
714	4.96E-3	40.97	201.98	203.58	240.95	196.61	233.97
758	4.92E-3	41.30	201.98	206.91	243.01	199.19	235.29
806	4.90E-3	41.47	201.98	208.60	242.93	199.92	234.25
847	4.88E-3	41.64	201.98	210.31	243.39	200.81	233.88
909	4.86E-3	41.81	201.98	212.05	243.26	201.20	232.42
943	4.84E-3	41.98	201.98	213.80	244.26	202.22	232.68
1000	4.82E-3	42.16	201.98	215.58	244.68	202.67	231.77

APPENDIX I

VELOCITY VS. FREQUENCY FOR 3M RECORDING MEDIUM

Table IV

Velocity vs. Frequency for 3M Recording Medium

TYPE OF WEB:	3M RECORDING MEDIUM	
WIDTH OF WEB:	0.1365	m
DENSITY OF WEB	0.1154	Kg/m^2
THICKNESS OF WEB:	7.94E-05	m
YOUNG'S MODULUS:	3.45E+9	Pa
SPEED OF SOUND:	331.6	m/sec
DENSITY OF AIR:	1.21	Kg/m^3
MOMENT OF INERTIA:	5.695E-15	m^4
TENSION OF WEB:	525.378	N/m^2

	MEMBRANE MODEL WITH AIR-LOADING	TENSIONED-PLATE WITH AIR-LOADING
VELOCITY m/sec	FREQUENCY Hz	FREQUENCY Hz
1	0.00	0.00
2	0.01	0.01
3	0.02	0.02
4	0.05	0.05
5	0.09	0.09
6	0.16	0.16
7	0.25	0.25
8	0.38	0.38
9	0.54	0.54
10	0.75	0.75
11	1.00	1.00
12	1.31	1.31
13	1.67	1.67
14	2.10	2.10
15	2.61	2.61
16	3.19	3.19
17	3.85	3.85
18	4.61	4.61

19	5.47	5.47
20	6.44	6.44
21	7.53	7.53
22	8.75	8.75
23	10.12	10.12
24	11.63	11.63
25	13.32	13.32
26	15.18	15.18
27	17.24	17.24
28	19.51	19.51
29	22.02	22.01
30	24.77	24.77
31	27.80	27.80
32	31.14	31.14
33	34.80	34.80
34	38.82	38.82
35	43.24	43.24
36	48.10	48.10
37	53.43	53.43
38	59.30	59.30
39	65.76	65.76
40	72.87	72.87
41	80.72	80.72
42	89.39	89.38
43	98.98	98.97
44	109.62	109.61
45	121.44	121.43
46	134.62	134.60
47	149.36	149.33
48	165.89	165.85
49	184.51	184.45
50	205.59	205.51
51	229.57	229.46
52	257.03	256.86
53	288.67	288.43
54	325.44	325.09
55	368.58	368.05
56	419.75	418.94
57	481.26	479.98
58	556.39	554.29
59	649.96	646.40
60	769.38	763.00
61	926.64	914.47
62	1142.48	1117.27
63	1456.18	1398.11
64	1952.29	1799.05
65	2851.97	2375.42
66	4976.64	3161.45
67	16078.55	4112.46

67.1	20454.48	4212.79
67.2	28024.13	4313.66
67.3	44292.23	4414.97
67.4	104497.33	4516.65
67.41	120857.02	4526.83
67.42	143269.89	4537.02
67.43	175858.08	4547.21
67.44	227585.77	4557.40
67.45	322324.20	4567.60
67.46	551889.09	4577.80
67.47	1914159.07	4588.00
68		5130.40
69		6146.19
70		7134.35
70.1		7231.42
70.2		7328.16
70.3		7424.60
70.4		7520.72
70.5		7616.54
70.6		7712.06
70.7		7807.28
70.8		7902.21
70.801		7903.16
70.802		7904.10
70.8021		7904.20
70.8022		7904.29
70.80221		7904.30
70.80222		7904.31
70.80223		7904.32
70.80224		7904.33
70.80225		7904.34
70.80226		7904.35
70.80227		7904.36
70.80228		7904.37
70.80229		7904.38
70.80230		7904.39
70.80231		7904.39
70.80231		49664.79
70.80241		49665.38
70.80251		49665.98
70.80261		49666.58
70.80271		49667.17
70.80281		49667.77
70.80291		49668.36
70.80301		49668.96
70.80311		49669.55
70.80321		49670.15

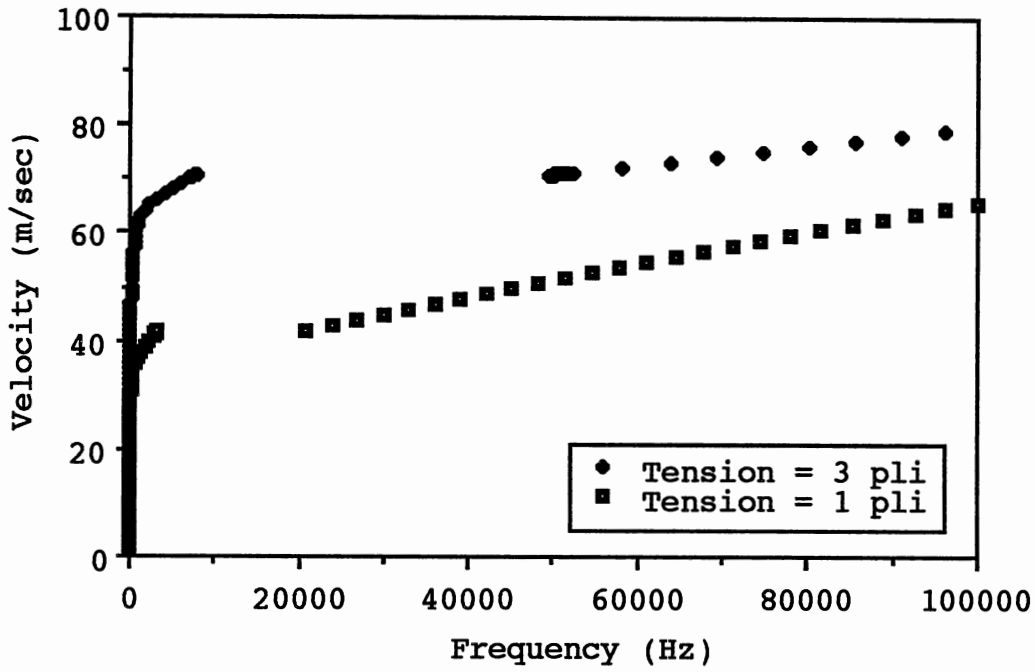

Figure 40. Predicted Velocities by Tensioned-Plate Model with Various Frequencies

APPENDIX J

VELOCITIES DUE TO AIR-LOADING EFFECT

Table V

Velocities due to Air-Loading Effect

TYPE OF WEB:	3M RECORDING MEDIUM	
WIDTH OF WEB:	0.1365	m
DENSITY OF WEB	0.1154	Kg/m^2
THICKNESS OF WEB:	7.94E-05	m
YOUNG'S MODULUS:	3.45E+09	Pa
SPEED OF SOUND:	331.6	m/sec
DENSITY OF AIR:	1.21	Kg/m^3
MOMENT OF INERTIA:	5.695E-15	m^4
TENSION OF WEB:	875.63	N/m^2

DISTANCE BETWEEN PLATE AND WEB	TIME OF FLIGHT	VELOCITY
m	sec	m/sec
8.89E-04	2.44E-03	42.42
1.02E-03	2.43E-03	42.59
1.14E-03	2.40E-03	43.13
1.27E-03	2.39E-03	43.31
1.40E-03	2.37E-03	43.67
1.52E-03	2.36E-03	43.86
1.65E-03	2.35E-03	44.04
1.78E-03	2.35E-03	44.04
1.91E-03	2.34E-03	44.23
2.03E-03	2.33E-03	44.42
2.16E-03	2.33E-03	44.42
2.48E-03	2.32E-03	44.61
2.79E-03	2.33E-03	44.42
3.11E-03	2.33E-03	44.42
3.43E-03	2.32E-03	44.61
4.06E-03	2.32E-03	44.61
4.70E-03	2.31E-03	44.81
5.33E-03	2.31E-03	44.81
5.97E-03	2.31E-03	44.81
7.24E-03	2.31E-03	44.81
8.51E-03	2.30E-03	45.00
1.10E-02	2.29E-03	45.20

1.36E-02	2.28E-03	45.40
1.99E-02	2.28E-03	45.40
2.63E-02	2.28E-03	45.40
9.27E-02	2.28E-03	45.40

APPENDIX K

SAMPLE CALCULATION FOR STIFFNESS

The Mead 80 LB. signature dull is used as the testing material. Its density and thickness are fixed parameters. The length and width of the web is selected.

Fixed parameters:

$$\begin{cases} \sigma_2 = 0.1213\ \text{Kg/m}^2 \\ h = 98.4\mu\text{m} \end{cases} \quad \text{or} \quad \begin{cases} l = 2.999\ \text{in} \\ b = 0.395\ \text{in} \end{cases} \tag{K.1}$$

Measured Data from Figure 41:

$$\begin{cases} X_1 = 681.25\ \text{mV} \\ X_2 = 475\ \text{mV} \\ \tau_d = 152\ \text{ms} \end{cases} \tag{K.2}$$

Based on the measured data, the damping frequency of the web can be determined by

$$f_d = \frac{1}{\tau_d} \quad \Rightarrow \quad f_d = 6.5789\ \text{Hz} \tag{K.3}$$

and the damping coefficient can be calculated by

$$\ln\left(\frac{X_1}{X_2}\right) = \frac{2\pi\zeta}{\sqrt{1-\zeta^2}} \quad \Rightarrow \quad \zeta = 0.0462 \tag{K.4}$$

Therefore,

$$f_n = \frac{f_d}{\sqrt{1-\zeta^2}} \quad \Rightarrow \quad f_n = 6.586\ \text{Hz} \tag{K.5}$$

Calculate the web's moment of inertia and mass:

$$I = \frac{1}{12}bh^3 \quad \Rightarrow \quad I = 7.94 * 10^{-16}\ m^4 \tag{K.6}$$

$$m = \sigma_2 b\ell \quad \Rightarrow \quad m = 9.2704 * 10^{-5}\ Kg \tag{K.7}$$

The natural frequency for a cantilever beam is

$$f_n = \left(\frac{3.515}{2p}\right)\sqrt{\frac{EI}{m\ell^3}} \tag{K.8}$$

Therefore, the Young's modulus for Mead 80 LB. signature dull is

$$E = 7.14 * 10^9\ N/m^2 \tag{K.9}$$

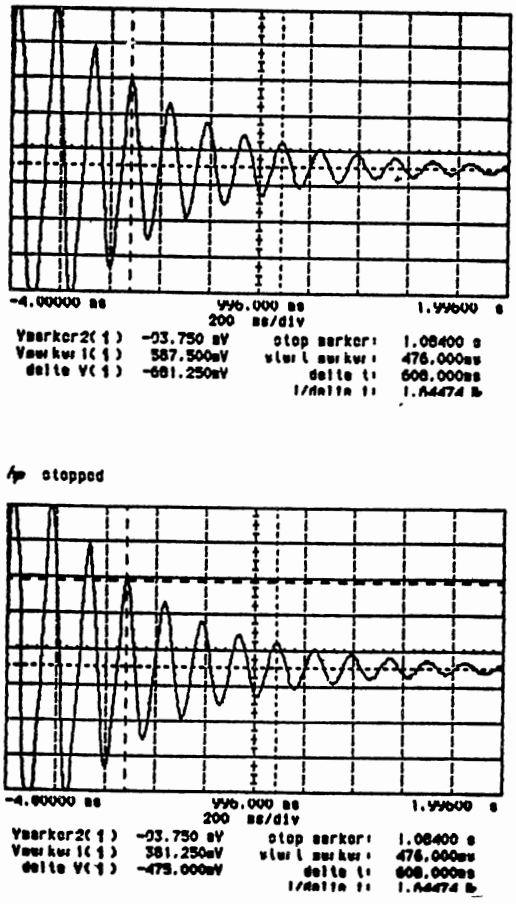

Figure 41. Free Vibration Signals of Mead 80 LB. Signature Dull Detected by OPTEK Sensor

VITA

Suefen Chen

Candidate for the Degree of

Doctor of Philosophy

Thesis: WAVE PROPAGATION IN DISPERSIVE WEB MEDIA

Major Field: Mechanical Engineering

Biographical:

Personal Data: Born in Chi-Lung, Taiwan, Republic of China, November 17, 1962, the daughter of Tsann-Ching and Hsiao-Chin C. Chen. Married to Minter Cheng on January 7, 1989.

Education: Graduated from Chung-Shan Girls' High School, Taipei, Taiwan, in May, 1980; received Bachelor of Science Degree in Chemical Engineering from Chinese Culture University in June, 1984; received Master of Science degree in Bioenvironmental Engineering from Oklahoma State University in July, 1986; completed requirements for the Doctor of Philosophy degree at Oklahoma State University in December, 1992.

Professional Experience: Research Assistant, Department of Chemical Engineering, Oklahoma State University, January, 1987, to August, 1987 and May, 1988 to June, 1988; Teaching Assistant, Department of Chemical Engineering, Oklahoma State University, September, 1987, to May, 1988 and September, 1988 to December, 1988; Teaching Assistant, Department of Mechanical Engineering, Oklahoma State University, January, 1989, to July, 1990; Research Assistant, Department of Mechanical Engineering, Oklahoma State University, June, 1990, to present.